

RESEARCH

Open Access



Cocultured amniotic stem cells and cardiomyocytes in a 3-D acellular heart patch reduce the infarct size and left ventricle remodeling: promote angiogenesis in a porcine acute myocardial infarction model

Muhammad Arza Putra^{1*} , Normalina Sandora^{2*} , Tri Wisesa Soetisna³, Tyas Rahmah Kusuma², Nur Amalina Fitria², Benati Karimah², Deni Noviana⁴, Gunanti⁴, Pribadi Wiranda Busro⁵, Supomo⁶ and Idrus Alwi⁷

Abstract

Background Acute myocardial infarction (AMI) induces significant myocardial damage, ultimately leading to heart failure as the surrounding healthy myocardial tissue undergoes progressive deterioration due to excessive mechanical stress.

Methods This study aimed to investigate myocardial regeneration in a porcine model of AMI using an acellular amniotic membrane with fibrin—termed an amnion bilayer (AB) or heart patch—as a cellular delivery system using porcine amniotic stem cells (pASCs) and autologous porcine cardiomyocytes (pCardios). Fifteen pigs (aged 2–4 months, weighing 50–60 kg) were randomly assigned to three experimental groups (n=5): control group (AMI induction only), pASC group (pASC transplantation only), and coculture group (pASC and pCardio transplantation). AMI was induced via posterior left ventricular artery ligation and confirmed through standard biomarkers. After eight weeks, histological and molecular analyses were conducted to assess myocardial regeneration.

Results Improvement in regional wall motion abnormality (RWMA) was observed in 60% of the coculture group, 25% of the pASC group, and none in the control group. Histological analysis of the control group revealed extensive fibrosis with pronounced lipomatosis, particularly at the infarct center. In contrast, pASC and coculture groups exhibited minimal fibrotic scarring at both the infarct center and border regions. Immunofluorescence analysis demonstrated positive α -actinin expression in both the pASC and coculture groups, with the coculture group displaying sarcomeric structures—an organization absent in control group. RNA expression levels of key cardiomyogenic markers, including cardiac troponin T (cTnT), myosin heavy chain (MHC), and Nkx2.5, were significantly elevated in the treatment groups compared to the controls, with the coculture group exhibiting the highest MHC expression. The expression of c-Kit was also increased in both treatment groups relative

*Correspondence:

Muhammad Arza Putra
putramuhammadarza@gmail.com
Normalina Sandora
normalinasandora@gmail.com

Full list of author information is available at the end of the article



© The Author(s) 2025. **Open Access** This article is licensed under a Creative Commons Attribution-NonCommercial-NoDerivatives 4.0 International License, which permits any non-commercial use, sharing, distribution and reproduction in any medium or format, as long as you give appropriate credit to the original author(s) and the source, provide a link to the Creative Commons licence, and indicate if you modified the licensed material. You do not have permission under this licence to share adapted material derived from this article or parts of it. The images or other third party material in this article are included in the article's Creative Commons licence, unless indicated otherwise in a credit line to the material. If material is not included in the article's Creative Commons licence and your intended use is not permitted by statutory regulation or exceeds the permitted use, you will need to obtain permission directly from the copyright holder. To view a copy of this licence, visit <http://creativecommons.org/licenses/by-nc-nd/4.0/>.

to the control. Conversely, apoptotic markers p21 and Caspase-9 were highest in the control group, while coculture group exhibited the lowest p53 expression.

Conclusion Epicardial transplantation of an acellular amniotic heart patch cocultured with cardiomyocytes and pASCs demonstrated superior cardiomyogenesis after eight weeks compared to pASC transplantation alone or control conditions. The coculture system was found to enhance the cardiac regeneration process, as evidenced by improved RWMA, distinct sarcomeric organization, reduced fibrotic scarring, and lower apoptotic gene expression.

Keywords Myocardial infarction, Animal models, Cardiomyogenesis, Amnion epithelial stem cells, Cardiomyocytes, Amnion bilayer 3-D scaffold, Heart patch

Introduction

Heart disease is a major global health concern, responsible for approximately 17.6 million deaths annually, with projections indicating an increase to 23 million deaths by 2030 [1]. In Indonesia, heart disease accounts for 13.3% of total mortality, according to the Sample Registration System (SRS), resulting in an estimated 651,481 deaths annually [2]. The financial burden is significant, with healthcare expenditures for heart disease-related conditions reaching USD 943 million—21.8% of total healthcare spending in 2017 [3, 4]. Despite these high expenditures, outcomes remain poor, with a five-year survival rate of only 50% [5].

Acute myocardial infarction (AMI) is primarily caused by coronary artery obstruction, leading to ischemic cardiomyopathy and irreversible cardiomyocyte death. The infarcted area undergoes a progressive process, beginning with an inflammatory phase within the first few hours to one week, characterized by inflammatory cell infiltration and protease activity [6, 7]. This is followed by a fibrotic phase lasting several weeks and, finally, a remodeling and scar maturation phase that can persist for months [7]. Severe AMI can result in immediate cardiac systolic dysfunction, especially when multiple coronary vessels are involved or if the patient experiences recurrent infarctions [5]. A large infarct can lead to significant structural and functional impairment of the ventricular wall, as the remaining healthy cardiomyocytes are subjected to excessive stress in an attempt to compensate for the damaged myocardium [8].

Each heart attack leads to the loss of up to 10 billion cardiomyocytes, and the body's natural regenerative mechanisms are insufficient to restore heart function, even with revascularization [9]. While cardiomyocytes can be replaced through endogenous mechanisms such as proliferation of existing cardiomyocytes, progenitor cells, or extracardiac stem cells, these processes are inadequate for effective myocardial repair [10]. Research has shown that cardiomyocyte turnover in adults is extremely limited, with a lifelong renewal rate of less than 50%, decreasing from 1% per year at age 20 to just 0.3% per year by age 75 [11]. Consequently, relying solely on

the body's natural repair mechanisms to restore heart function after infarction is ineffective.

Heart failure is a progressive and often terminal condition that frequently necessitates heart transplantation for survival. However, the availability of donor hearts is extremely limited. While survival rates following heart transplantation have improved, they continue to decline over time, with survival rates of 72.6%, 56.7%, and 34.9% at 2, 5, and 10 years post-transplantation, respectively [12, 13]. Studies indicate that female heart failure patients tend to have a longer survival rate (up to 3.2 years) compared to males (1.7 years) [14]. Furthermore, despite adherence to standard heart failure treatments, cardiac remodeling continues to progress, ultimately leading to end-stage heart failure [15]. This highlights the urgent need for alternative therapies that can prevent heart failure and promote myocardial regeneration.

In response to this challenge, extensive research has focused on regenerative strategies for AMI. Cell-based therapies, with or without biomaterial scaffolds, have demonstrated promising results in both preclinical and clinical studies [16]. The most commonly studied cell types for myocardial regeneration include cardiac progenitor cells and pluripotent stem cells. A meta-analysis of 166 AMI studies in mice reported a 10.21% improvement in left ventricular ejection fraction four weeks after cell administration [17]. Additionally, three-dimensional biomaterial-based approaches, such as viable amnion membrane transplantation in rats [18] and CD56-positive cell-layer patches combined with polymer (poly-N-isopropylacrylamide) and fibrin glue [16], have shown significant improvement in cardiac function.

This study investigates the regenerative potential of autologous cardiomyocytes in combination with amniotic cells. Amniotic cells were chosen due to their availability, minimal ethical concerns, and beneficial properties, including pluripotency, low immunogenicity, and regenerative potential [19, 20]. To enhance cell retention, transepical delivery was performed using an acellular amniotic heart patch, while intramyocardial injections were administered via plasma fibrin.

Materials and methods

All procedures in this study were conducted in accordance with the ethical guidelines for animal research outlined in the Declaration of Helsinki. The protocols were reviewed and approved by the Animal Experimentation Unit Ethical Committee of the Institut Pertanian Bogor, Indonesia (approval number 158/KEH/SKE/XII/2019). Additionally, protocols for human amnion collection were reviewed and approved by the Ethics Committee of the Faculty of Medicine, University of Indonesia (Approval Number KET-1307/UN2.F1/ETIK/PPM.00.02/2019).

Seventeen pigs (*Sus scrofa domestica*) in total were used in this study, sourced from a local slaughterhouse. Fifteen pigs were allocated to the experimental study and divided into three groups ($n = 5$ per group). All pigs were of the same breed, aged 2–4 months, and weighed 57.85 ± 7.58 kg at the time of intervention. One full-term pregnant pig was obtained for pASC donor, one healthy pig was used for histology and PCR control. The experimental groups were as follows: (i) the control group, which received no treatment after infarction; (ii) the pASC group, which received porcine adipose-derived stem cells [21] delivered via a heart patch and injection; and (iii) the co-culture group, which received a combination of pASC and porcine self-cardiomyocytes delivered via a heart patch and injection. One pig in the control group was excluded due to ventricular fibrillation immediately after ligation of the PLV (posterolateral ventricular branch) for infarct modeling (Fig. 1).

Due to challenges posed by the COVID-19 pandemic, each group consisted of five samples, the minimum required for non-parametric statistical analysis. Initially, three batches of pigs were acquired throughout the study; however, two earlier batches died during acclimatization due to pneumonia. To address this issue, the remaining pigs were housed individually. Additionally, one pregnant pig was used as the donor for pASC.

Isolation of porcine cardiomyocytes (pCardios)

Cardiomyocytes were provided and given to the same pig or autologous source, harvested from the right atrial appendage once the heart had been exposed after thoracotomy. The tissue was taken from this part as this area is not actively involved in heart pumping; therefore, it is not harmful to the subject. The piece of heart tissue was immediately placed in a warmed transport medium (37 °C) containing Dulbeccos' modified eagle medium (DMEM, Gibco, USA) supplemented with 10% (v/v) fetal bovine serum (FBS, Gibco, USA) and 3% (v/v) antibiotic/antimycotic (ABAM, Gibco, USA), and delivered to the laboratory under the optimal conditions described in our previous study [22]. Single cardiomyocytes were isolated, as described in our previous publication [23]. Briefly, the heart tissue was minced to a size of $2 \times 2 \times 2$ mm³, washed three times in Ca⁺⁺Mg⁺⁺-free Dulbecco's phosphate buffer solution (DPBS, Sigma), placed in a gentleMACS C-tube (Miltenyi Biotec, Germany), and treated with 250 U mL⁻¹ collagenase type V (Thermo Fisher Scientific, USA) and 4 U mL⁻¹ proteinase XXIV (Thermo Fisher Scientific, USA) to prepare a 3 mL

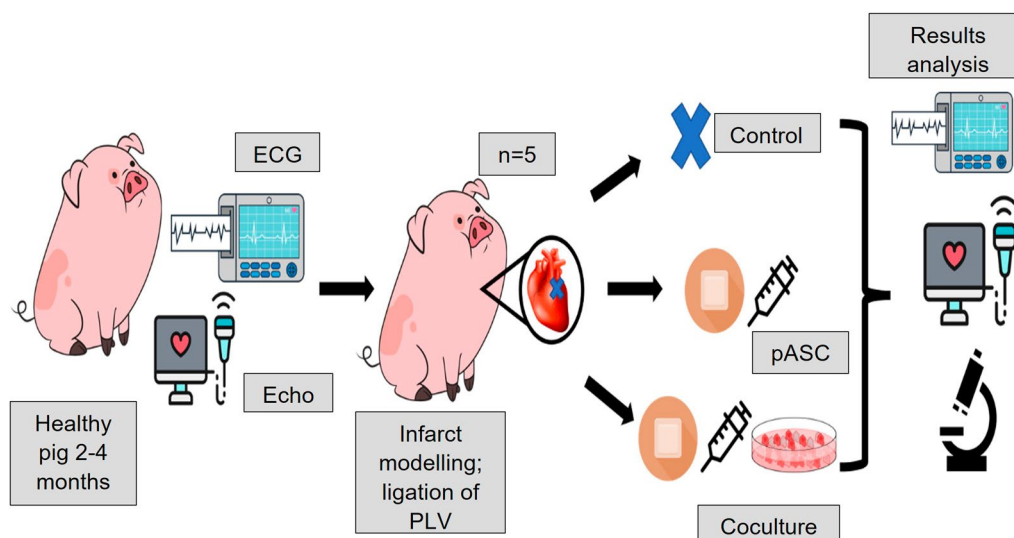


Fig. 1 Study design. A total of 17 pigs were used in this study. Sixteen pigs were randomly assigned to three experimental groups ($n = 5$ per group), while one pig served as a normal control without any intervention. Additionally, a mature pregnant pig was used for pASC harvesting. The total duration of the experiment was ten weeks

suspension. The C-tube was then inserted upside-down into a gentleMACS™ Octo Dissociation Sleeve with Heater (Milltenyi Biotec, Germany), fastened with the heater case, and run using the recommended program for the neonatal heart dissociation kit (NHDK) at 37 °C for 60 min. Once completed, the suspension was neutralized by adding a 2 × volume of complete culture medium containing DMEM supplemented with 10% (v/v) FBS and 1% (v/v) ABAM, the cells were separated using a 70 µm cell strainer (Biologix, Nigeria) and collected by centrifugation at 600×g for 10 min at 25 °C. Viable cells were distinguished from dead cells using the Trypan blue assay and visualized using an Avio A1 Brightfield microscope at 100× magnification (Carl Zeiss, Germany), and the number of isolated viable cells is presented as the number of unstained cells per mg tissue weight. All specimens for cell isolation transported to the laboratory were tested for sterility by incubating one mL of the transport medium in nutrient broth (HiMedia Laboratories, India) for 14 days, followed by spreading on blood agar and Sabouraud dextrose agar and incubation at 37 °C for 14 days. All procedures were performed under aseptic conditions unless otherwise stated.

Isolation of porcine amnion stem cells (pASCs)

One pig at 14 weeks gestation was prepared for cesarean section to obtain the amniotic stem cells, which were used throughout the study. The amnion membrane was transported aseptically to the laboratory at 4 °C within 30 min in a transport medium containing Hank's balanced salt solution (HBSS, Gibco, USA) supplemented with 10% (v/v) FBS and 3% (v/v) ABAM. Once the amnion membrane arrived at the laboratory, one mL of the transport medium was subjected to bioburden analysis. The amnion membrane was then washed in Ca⁺⁺Mg⁺⁺-free DPBS (Sigma, USA), separated from the chorion, placed on a plate with the fetal side facing upward, and incubated with 0.25% (v/v) Trypsin-EDTA (Thermo Fisher Scientific, USA) for 60 min at 37 °C. Then, 1× culture medium was added, the surface area was scraped thoroughly with a blunt blade, and the cells were collected and suspended. The amnion membrane was then flipped over so that the maternal side faced upward and incubated with 2 mg/mL collagenase type I (Thermo Fisher Scientific, USA) and 66.6 IU/mL hyaluronidase in DMEM (4.5 g/L glucose, Sigma, USA) for 60 min at 37 °C. The digestion was stopped by adding 2× culture medium, and then the entire membrane was scraped using a blunt blade; the collected cell suspension was then pooled in a centrifugation tube, filtered through a 100 µm cell strainer (Biologix, China), and harvested by centrifugation at 150×g for 10 min. All of the cells were used in this study and analyzed for viability using the

Trypan blue assay, and cell viability was measured as the number of viable cells mL⁻¹ before use.

Cell characterization using flow cytometry

All the isolated cells, pCardio cells and pASCs were characterized using a BD FACS Aria™ III flow cytometer (BD Bioscience, USA), and the data were analyzed using BD FACS Diva 8.0.2 (BD Bioscience, USA) to identify cell types. Cardiomyocytes that expressed cTnT (FITC; Santa Cruz Biotechnology, USA) [24]—isotype IgG2a kappa (FITC; Abcam, UK), intercellular adhesion molecule 1 (ICAM/CD54) (PE; Milltenyi, Biotec, Germany) with IgG1 kappa (PE; Santa Cruz Biotechnology, USA), platelet endothelial cell adhesion molecule 1 (PECAM-1/CD31) (FITC; BD Bioscience, USA) with IgG1 kappa (FITC; Stemcell TM, USA), vascular cell adhesion molecule 1 (VCAM-1/CD 106) (PE; BioLegend, USA) with IgG1 kappa (PE; Santa Cruz Biotechnology, USA) [25], or stem cell growth factor receptor (cKit/CD117) (PE; Miltenyi Biotec, Germany) with IgG1 kappa (PE; Santa Cruz Biotechnology, USA) were considered as pCardios. pASCs were identified by their pluripotency, i.e., their expression off T-cell receptor alpha (TRA-1-60) (PE; Santa Cruz Biotechnology, USA) with IgM (PE; mouse monoclonal antibody; BioLegend, USA), stage-specific embryonic antigen-4 (SSEA-4) (813-70) (FITC; Santa Cruz Biotechnology, USA) with IgG3 (FITC; mouse monoclonal antibody; Santa Cruz Biotechnology, USA), Nanog (A-11) (PE; Santa Cruz Biotechnology, USA) with IgG1 kappa (PE; mouse monoclonal antibody; Santa Cruz Biotechnology, USA), Oct-3/4 FITC (C-10) (Santa Cruz Biotechnology, USA) with IgG2b (FITC; mouse monoclonal antibody; BioLegend, USA). The procedure for flow cytometry is presented in the Supplement 1.

Preparation of an acellular human amnion bilayer as a heart patch

The acellular human amnion used for the heart patch was collected from amnion membrane of a full-term pregnancy through caesarean, non-reactive to Cytomegalovirus, Hepatitis A and B, Human Immunodeficiency Virus/HIV. Once the consent was obtained, the amnion was transported in PBS with Ca⁺⁺Mg⁺⁺ (Gibco, USA), added with 3% (v/v) ABAM at 4 °C, and stored at -80 °C until processing. The amnion was decellularized using serial of 0.05% SDS (w/v) and 0.1% Triton-X (v/v) washes, and the acellularity was verified using H&E, DAPI staining and DNA quantification (Qiagen, USA). The acellular amnion was then overlaid with fibrin. Once settled, the cytotoxicity of the acellular heart patch was tested by two methods: the extract and contact assays. Briefly, acellular heart patches were incubated in a culture medium containing DMEM

supplemented with 10% (v/v) platelet-rich plasma (PRP) and 1% ABAM for 3 days, followed by ATP analysis using ATPlite assay (PerkinElmer, USA), according to the manufacturer. The ATP counts were quantified using Varioskan™ LUX Multimode Microplate Reader (Thermo Fisher, USA). For the contact assay, acellular heart patches were placed in culture flasks, and human AECs were seeded around them. The culture was then observed for 7 days. Sterility was assessed during and after the decellularization process, also to the heart patch. These all showed no bacterial or fungal growth detected.

Seeding heart patches with cells

Preparation and seeding were performed as described in our previous study [26]. The amnion bilayer was blotted dry and seeded with cells at a density of 5×10^5 cells per cm^2 . The diameter of the heart patch was 4 cm; therefore, the total number of cells used to seed the patch was 6.5×10^6 cells. An equal number of cells were also prepared for the PRP suspension [27]. As described in our previous study, pASCs and pCardios were cultured at a ratio of 6:1 (23) for the coculture group. Briefly, (i) In preparation for the pASC group, 6.5×10^6 cells of pASCs were seeded onto the heart patch. Another 6.5×10^6 pASC cells were also suspended into 1.35 mL of PRP for intracardial-muscular injection (aliquotes into nine injections). (ii) Preparation for the cocultured group: the pASCs were mixed with pCardio at the ratio of 6:1 to make a total of 6.5×10^6 cells, then seeded onto a heart patch. A similar composition was also used to suspend in PRP. All cells for transplantation were suspended in sterile NaCl 0.9% (v/v) and maintained at 37 °C.

Animal handling

A total of sixteen large white domestic pigs weighing 50–70 kg and aged 2–4 months were selected for the study, were obtained from a local slaughterhouse Kuningan Farm, West Java and were from a single litter. The pigs were initially acclimated for seven days once they arrived at the laboratory of the Institut Pertanian Bogor Veterinary Hospital. The pigs were fed and given access to water ad libitum with standard pellets and clean water. They were randomly assigned to one of the three experimental groups: (i) Five pigs for the control group (AMI induction without treatment), but one was excluded due to ventricular tachycardia immediately after thoracotomy, (ii) five pigs for the pASCs group (injected with PRP and heart patch containing pASC), and (iii) five pigs for the coculture group (injected with PRP and heart patch containing pASC and pCardio). One healthy pig that received no intervention served as a negative control, and one pregnant pig for the

pASC donor. The number of pigs was limited due to the difficulty of maintaining the health of those animals during the COVID-19 pandemic.

Anesthesia and thoracotomy

The pigs were initially weighed and then deeply sedated using 2 mg kg^{-1} BW Xylazine (Randlab, Australia), 20 mg kg^{-1} BW Ketamine (Agrovet Market, Canada) intramuscular, and 0.05 mg kg^{-1} BW Atropin sulfate (ETHICA Industri Farmasi, Indonesia) intravenous for anaesthetic induction. After that, 5 mg kg^{-1} BW Propofol (Finusolprima Farma International, Indonesia) was given intravenously prior to the insertion of an endotracheal tube (ETT; no. 6 and no. 6.5), which was placed through the fifth tracheal ring (tracheostomy). The sedation was maintained by inhalation of Isoflurane 2–4% (Mersifarma Tirmaku Mercusana, Indonesia), with oxygen and nitrogen supply through RWD Vet Anesthesia R640-S1 ventilator (RWD Life Science, China), 60 × per minute.

All clinical data collected before thoracotomy, such as chest X-rays, ECG and Echocardiography, were recorded using RV-32 A (Dawei, China), Fukuda ME C120 (Fukuda Denshi, Japan), and Chison EBit60 VET Ultrasound (Chison Medical Imaging, China), respectively. Blood serum was collected to determine cardiac enzyme levels before and after the interventions. Thoracotomy was performed once the pig was heavily sedated using an intravenous bolus of 0.02–0.05 mg kg^{-1} BW Fentanyl (Mahakam Beta Farma, Indonesia); briefly, the rib cages were cut at the sixth intercostal space to expose the anterior face of the heart. Once the heart was revealed, about $0.5 \times 1 \times 1 \text{ cm}^3$ of myocardial tissue was harvested from the auricle of the right atrium for cardiomyocyte isolation. AMI was induced by permanent ligation of the left circumflex artery (PLV), tied at one cm distal to the sulcus atrioventricular with a polypropylene suture (Premilene no. 6–0; B. Braun, Germany), marked with PTFE polymer pledgets (Covidien, USA). AMI was indicated by the darkening of the myocardium in the region of interest (left ventricular wall), ST elevation, and increased serum cardiac troponin T (cTnT) and creatinine kinase-myocardial band (CK-MB) levels. After 60 min of ligation, the pigs were coin-tossed to decide the grouping. Initially, PRP loaded with or without cells was injected at the border surrounding the darkened area (nine injections of 150 μL PRP), then the darkened area was covered with a heart patch with or without cells, stitched with six knots of a 6.0 polypropylene suture to mark the infarct area. After the intervention, all the pigs were housed, fed and given water ad libitum with standard food pellets and were observed for 6–8 weeks (mean 7.46 ± 10.5 weeks).

Termination and specimen collection

The pigs were euthanased according to the exsanguination method of the American Veterinary Medical Association; Guidelines for the Euthanasia of Animals: 2020 Edition [28]. Briefly, the pig was heavily sedated with intramyocardial injections of 2 mg kg⁻¹ BW Xylazine and 20 mg kg⁻¹ BW Ketamine, intravenous injections of 0.04 mg kg⁻¹ BW Atropin sulfate, 5 mg kg⁻¹ BW Propofol, and 0.02–0.05 mg kg⁻¹ BW Fentanyl. Once the clinical data and specimen punch biopsies were obtained, a cardioplegic solution (Ringerfundin B. Braun, Germany) was injected through the aorta. Gadolinium/Gadovist (Bayer, Germany) was given through the coronary artery for late gadolinium enhancement/LGE to allow magnetic resonance imaging (MRI) visualization of the infarct area. The heart was removed five minutes after injection and prepared for an MRI. After that, heart tissue was subsequently collected for histological specimens, as shown in Fig. 3a; each 5 × 5 mm, taken from 4 sites: the infarct center (no. 3), the left (no. 4) and right borders (no. 2), and a remote area (no. 1). The border was defined as the line between the area covered and the area not covered by the heart patch. The remote area was the right atrium wall, which was not affected by the ligation. All the histological specimens were preserved in 10% neutral-buffered formalin (Leica, Germany) 10% (v/v), and immediately processed after three days fixation. Samples for PCR were preserved in RNAlater solution (Thermo Fisher Scientific, USA), stored at 4 °C for one week and isolated the RNA using TRIzol™ Reagent (Thermo, USA) according to the manufacturer's instruction.

Analysis of the heart

Electrical conduction and its kinetics were recorded using ECG (Fukuda Alpha1000) and echocardiography (Chison Ebit 60, China). MRI was used to visualize the infarct area, and late gadolinium enhancement cardiac magnetic resonance (LGE-CMR) was used to visualize viable tissue at the left ventricular endocardium. MRI images were acquired at a median of 53.5 (50–57) days post-infarct. All imaging was performed on a 1.5-T scanner (PHILIPS, Ingenia, Germany) with an 18-channel body matrix coil and a 32-channel spine coil, and the data were converted into densitometry data using IntelliSpace Portal 9.0 software (PHILIPS, Germany). Protocol of ELISA to determine cardiac enzymes presented in Supplement 1.

Histological, immunohistochemical and immunofluorescence analysis

All specimens for histological analysis were processed automatically in a tissue processor (Leica, USA), embedded in paraffin, and sectioned at 5 μm thickness.

Paraffin blocks were stored in –20 °C, while tissue sections were stored at room temperature. Hematoxylin and eosin (H&E) (Scytek, USA) and Masson trichrome (Scytek, USA) staining were used to visualize tissue architecture. All immunohistochemical (IHC) protocols were performed with the biotin-avidin method; heat-induced epitope retrieval with 10 mM citric acid (pH 6; microwave at 95–100 °C, 10 min) was performed for α-SMA staining and incubation with proteinase K (Dako, Denmark) at 25 °C for 10 min was performed for collagen 1, collagen 3 and vWF staining. All antibodies against components of the extracellular matrix were incubated with the samples for one hour at 25 °C, except those against collagen 1 (1:100 dilution, Invitrogen, USA) and collagen 3 (1:50 dilution, Abcam, USA) [29], which were incubated with the samples overnight at 4 °C. Scar formation was investigated by assessing the presence of myofibroblasts by labelling against α-SMA (1:400 dilution, Sigma). Angiogenesis was indicated by vWF labelling (1:200 dilution, Dako, Denmark).

All sections subjected to histological and IHC staining were visualized using a brightfield microscope (Zeiss, Germany), and images were acquired using a Zeiss Axio Imager (Zeiss, Germany). Myocardial fibers were visualized by immunofluorescence (IF) staining for alpha-actinin (Alexa Fluor 555; 1:500, Invitrogen, USA) with biotin-avidin labelling. The sections were visualized using confocal microscopy ZEISS LSM 900 (Zeiss, Germany) at an excitation wavelength of 555 nm and an emission wavelength of 565 nm.

Real-time RT-qPCR analysis

In this study, gene expression was analyzed in RNA samples obtained from the punch biopsy according to Fig. 4a and stored at 4 °C in RNAlater solution (Gibco, USA) until all the samples were collected. The genes of interest (GOIs) related to cardiomyogenesis were α-actinin (which regulates the transcription of actin-binding protein) [30], cTnT (which generates troponin I to mediate the relaxation of striated muscles) [31], MHC, and Nkx2.5 [32]. The expression of other GOIs, such as the progenitor marker cKit, was also evaluated to determine the remaining pASCs to differentiate, and the expression of apoptosis-related genes such as p21, Caspase9 and p53 were also assessed [33, 34]. Procedure for PCR is presented in Supplement 1.

Data analysis

The result of infarct modelling was confirmed by the appearance of ST elevation in ECG. All histology and IHC data were presented as images. Characteristic data were presented as mean ± standard deviation. Numeric data such as cell counting, cellular characteristics/

flowcytometry, and PCR were presented as mean ± 95% C.I, analysed using one-way ANOVA, followed by a post hoc test using Tukey’s method to highlight the difference among the groups. For the nonparametric data, Kruskal–Wallis test was used.

Results

All pigs were 2–4 months old and weighed 57.85 ± 7.58 kg during the intervention period; 6 females (46.2%) and 7 males (53.8%) had statistically no differences in weight and sex among the groups. All pigs in the pASC and coculture group survived, while one pig in the control group died ligation of the PLV due to ventricular tachycardia during infarct modeling. The study flow and

characteristics of the experimental groups are presented in Fig. 1 and Table 1, respectively.

Confirmation of ligation-induced AMI

In our study, the data analysis of the heart collected before intervention was similar among all the pigs. Myocardial infarction was successfully induced in all pigs, as shown by the increase of serum cTnT (Fig. 2a) and CK-MB (Fig. 2b) after ligation of the PLV. The average cTnT level had increased from 6.24 ± 5.7 pg mL⁻¹ (95% CI: 0.00–33.79 pg mL⁻¹) pre-ligation to 479.28 ± 82.94 pg mL⁻¹ (95% CI: 429.16–529.40 mU mL⁻¹) after ligation (500-fold increment), and the average CKMB level was also increased from 6.15 ± 1.059 mU mL⁻¹ (95% CI: 3.13–8.52 mU mL⁻¹)

Table 1 Demographic data analysis of the subjects

Demographic	Control	pASC	Co-culture	p value*
Male	3 (75%)	2 (50%)	2 (40%)	0.568
Female	1 (25%)	2 (50%)	3 (60%)	
Weight (kg)	57.50 ± 3.70	61.25 ± 7.14	55.40 ± 10.24	0.554
Ages (weeks)	19.75 ± 1.71	20.50 ± 1.29	20.20 ± 3.11	0.898
Observation (weeks)	7.0 ± 0.816	7.75 ± 1.258	7.6 ± 1.14	0.601
Weight by the end of the study (kg)	76.25 ± 12.738	72.25 ± 4.113	71.40 ± 11.415	0.769

Normally distributed data were analyzed using the Shapiro–Wilk test, while the other needed to be normalized, then the differences were analyzed using one-way ANOVA, while the *p*-value less than 0.05 was considered significant. Data were presented as mean ± SD. The demographic differences were found not significant among all groups

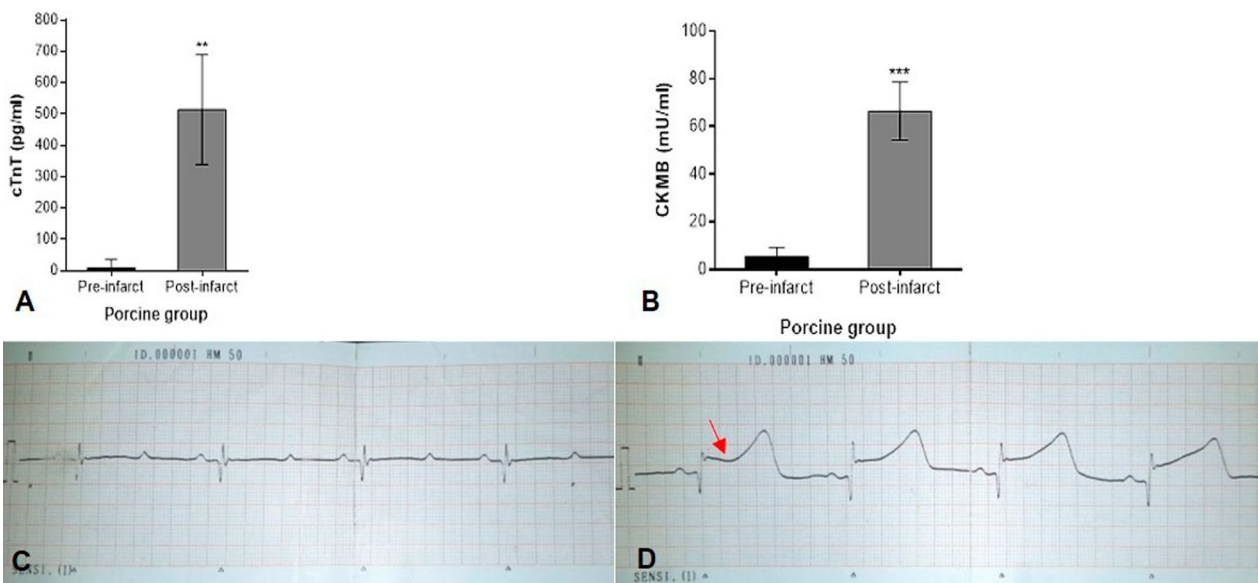


Fig. 2 Cardiac enzyme levels before and after ligation. **a** cTnT and **(B)** CK levels showed a significant increase following ligation compared to baseline (*p* = 0.002 and *p* = 0.001, respectively). Data are presented as mean values (*n* = 15) and analyzed using a paired Student’s t-test, with *p* < 0.05 considered statistically significant. **c, d** Electrocardiogram (ECG) recordings before and after ligation, respectively, reveal ST-segment elevation in lead II (red arrow), indicative of myocardial infarction

preligation to 69.26 ± 12.92 mU mL⁻¹ (95% CI: 61.45–77.72) (60-fold increment) ($p = 0.002$ and $p = 0.001$, respectively). ECG was performed before ligation (Fig. 1c) and after ligation (Fig. 1d). ECG revealed with ST elevation after the modelling (pointed by red arrow). The heart of all pigs enrolled into this study showed no differences among the groups ($p < 0.05$), had no abnormalities in the initial movement of the ventricular wall (average $69 \pm 16.81\%$ CI 95% 59.18–79.50), and the thickness of the left ventricular posterior wall (LVPW) was approximately 13.4 ± 3.97 mm (95% CI 11.01–15.81). The median interventricular septal wall (IVS) thickness was 12.4 mm (range 9.7–22.8 mm).

Cellular characteristics of the pASC and pCardio

The isolated pASCs were analysed for their mesenchymal properties and their pluripotency. It found that the pASCs had a low mesenchymal population; only CD 90 was 17.7%, while other mesenchymal epitopes were below 2%. The population of pluripotent cells was dominated by Nanog and Oct3/4, more than 50% each, although the SSEA-4 and TRA-1–60 were 38% and 17.5%, respectively. The pCardio showed to express cardiomyocyte phenotype as the population of cTnT cells was 48.1%, the cellular adhesion molecules/ICAM (2.8%), and very low in cardioprogenitor cells (cKit 0.5%). The flowcytometry data were presented in Supplement 2.

Biocompatibility of the heart patches

The heart patches were confirmed to be acellular and biocompatible presented in Supplement 3. Supplement 3A is the schema of the heart patch application on the pig heart, and Supplement 3B is the heart patch used in this study. The extract cytotoxicity assay (Supplement 3C) revealed no difference in the level of cellular ATP between the cells cultured with normal culture medium (cell only) and the cells cultured with acellular heart patch medium (amnion bilayer), indicating that the acellular amnion bilayers were not toxic. The ATP was presented as luminescence per second quantified using ATPlite assay by Perkin Elmer, USA. Supplement 3D and E are images of an acellular heart patch stained with H&E and DAPI, respectively, indicating that no nuclei were found. A contact toxicity assay was performed using human ASCs, and the results showed that the cells were able to adhere to the acellular heart patch (Supplement 3F, pointed by red arrow). Supplement 3 indicates that the heart patches were acellular and biocompatible. Supplement 3G and H are the cells of pASC and pCardio, respectively. All microscopy images were captured at 100 × mag.

Observation of the porcine heart and infarct area after 6–8 weeks

Intervention in this study was according to the grouping: heart patch with pASC or coculture cells stitched to the infarcted area, following Fig. 3a. The porcine were housed, fed and given water ad libitum for eight weeks, and the hearts of those porcine were collected once termination.

Table 2 indicates the ECG analysis of the pigs by the end of the experiment. After eight weeks of treatment, none of the pigs showed ECG abnormalities; however, echocardiography in the control group revealed left ventricular remodelling. The ejection fraction indicated the degree of remodelling, posterior wall thickness and inter-ventricular septal/IVS thickness. By the end of experiment, after 8 weeks infarction, the regional wall motion abnormalities (RWMAs) had improved in 60% of pigs in the coculture group and 25% of pigs in the pASC group. At the same time, no amelioration of RWMAs was observed in the control group. The EF did not differ among the groups ($p = 0.348$). There were no differences in the posterior and intraventricular wall thickness among the groups: ($p = 0.925$) and ($p = 0.322$), respectively.

Intervention in this study was according to the grouping, where the heart patch with or without cells was stitched to the infarcted area (Fig. 3a). The infarct area was measured using the MRI image converted into densitometry data. Figure 3b shows the infarct area in percentage at eight weeks after the intervention, indicating that the infarct area in the pASC and coculture groups was significantly smaller ($p = 0.0002$ and $p = 0.0003$, respectively) compared to the control group, no difference was found between the coculture and pASC groups ($p > 0.05$). Figure 3c–f show the data for the control group. The densitogram of the control group (Fig. 3d) showed dominant red scars that projected across the wall thickness, suggesting that IMA without treatment causes transmural infarction with very thick scars. The densitogram was parallel to the fibrosis appearance in the transversal cut across the infarct central, which scar was transmural (Fig. 3e), and Fig. 3f highlights the fibrosis. Figure 3g–j shows the pASC group, as Fig. 3h is the densitogram of the MRI image, displays light scars dominated with green and yellow areas, and appearance was parallel to other images. Figure 3k–n show the coculture group in which the densitogram exhibits a notable fine scar (Fig. 3l); although it had a small area of red mark, the fibrosis was also found in less than half of the wall thickness (Fig. 3m, n).

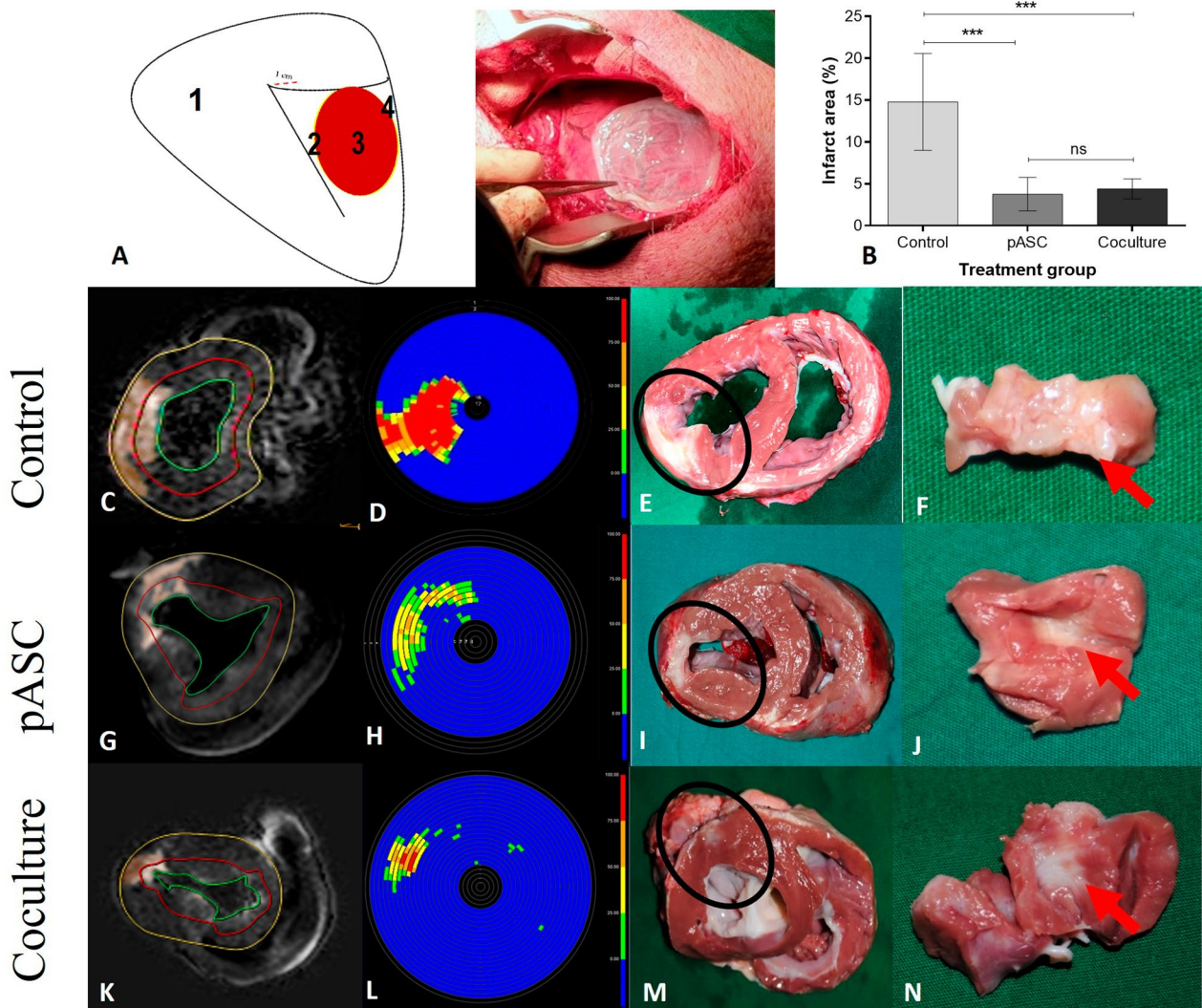


Fig. 3 Porcine Heart Following Myocardial Infarction Modeling and Heart Patch Treatment. **a** Representative image of the porcine myocardial infarction model following heart patch application. **b** Quantification of the infarct area after eight weeks of intervention, assessed using MRI measurements. Data were analyzed using one-way ANOVA for non-parametric comparisons, with $p > 0.05$ considered not significant. The figure presents MRI images of infarcted hearts (top left column), corresponding MRI interpretations (second column), and transverse sections of the heart at the infarct site, marked by a black circle (**e, i, m**) (transverse section at point three from Fig. 3a). The rightmost column (**f, j, n**) shows sections of the infarct center, indicated by red arrows. The top row represents the control group (**c–f**), the middle row corresponds to the pASC group (**g–j**), and the bottom row depicts the coculture group (**k–n**). The infarct area was visualized using late gadolinium enhancement (LGE) MRI contrast. Scar thickness and severity were mapped, converted into densitometry graphs, and analyzed using IntelliSpace Portal 9.0 (**d, h, l**)

Histology, immunohistochemistry, and immunofluorescence analysis

H&E-stained sections (Fig. 4 top left) from the control group showed massive scars stretching from the center of the infarct area to both border zones (Fig. 4b–d), the remote area (Fig. 4a, e, i); lipomatosis (indicated with a red arrow) and denatured collagen (indicated with a black arrow) were also observed in the center of the infarct area. The pASC group exhibited severe scars involving nearly half of the section but not the border

zones (Fig. 4f–h), while the cocultured cell group had minimal scars between fibers (Fig. 4j–l). The fibres appeared to be comparable to the remote sections (Fig. 4i). Scar severity was evaluated by Masson trichrome staining (Fig. 4 top right), which revealed that scars were widespread in the control group, and most of the muscle structures had disappeared (Fig. 4b–d). Consistent with what was observed by H&E staining, nearly half of the center of the infarct area in the pASC group showed scarring; however, scars were

Table 2 Heart function measurement using Echocardiography by the end of observation

Remodeling indicator	Control	pASC	Co-culture	p value*
Ejection fraction (%)	68.28 ± 8.64 (CI 95% 54.52–82.03)	68.33 ± 6.70 (CI 95% 57.66–78.99)	58.53 ± 14.92 (CI 95% 40.00–77.06)	0.348
Wall motion abnormalities				0.259
Improvement	0 (0%)	1 (25%)	(60%)	
No different	2 (50%)	2 (50%)	1 (20%)	
Deteriorated	2 (50%)	1 (25%)	1 (20%)	
Posterior wall thickness (mm)	12.58 ± 0.89 (CI 95% 11.15–14.00)	11.85 ± 2.15 (CI 95% 8.43–15.27)	11.82 ± 4.48 (CI 95% 6.26–17.38)	0.925
Interventricular septal wall thickness (mm)	13.03 ± 1.76 (CI 95% 10.23–15.82)	13.89 ± 0.83 (CI 95% 12.57–15.21)	11.7 ± 2.82 (CI 95% 8.19–15.21)	0.322

Data were analyzed using one-way ANOVA and Kruskal–Wallis for the categorical grouping, with $p < 0.05$ considered significant

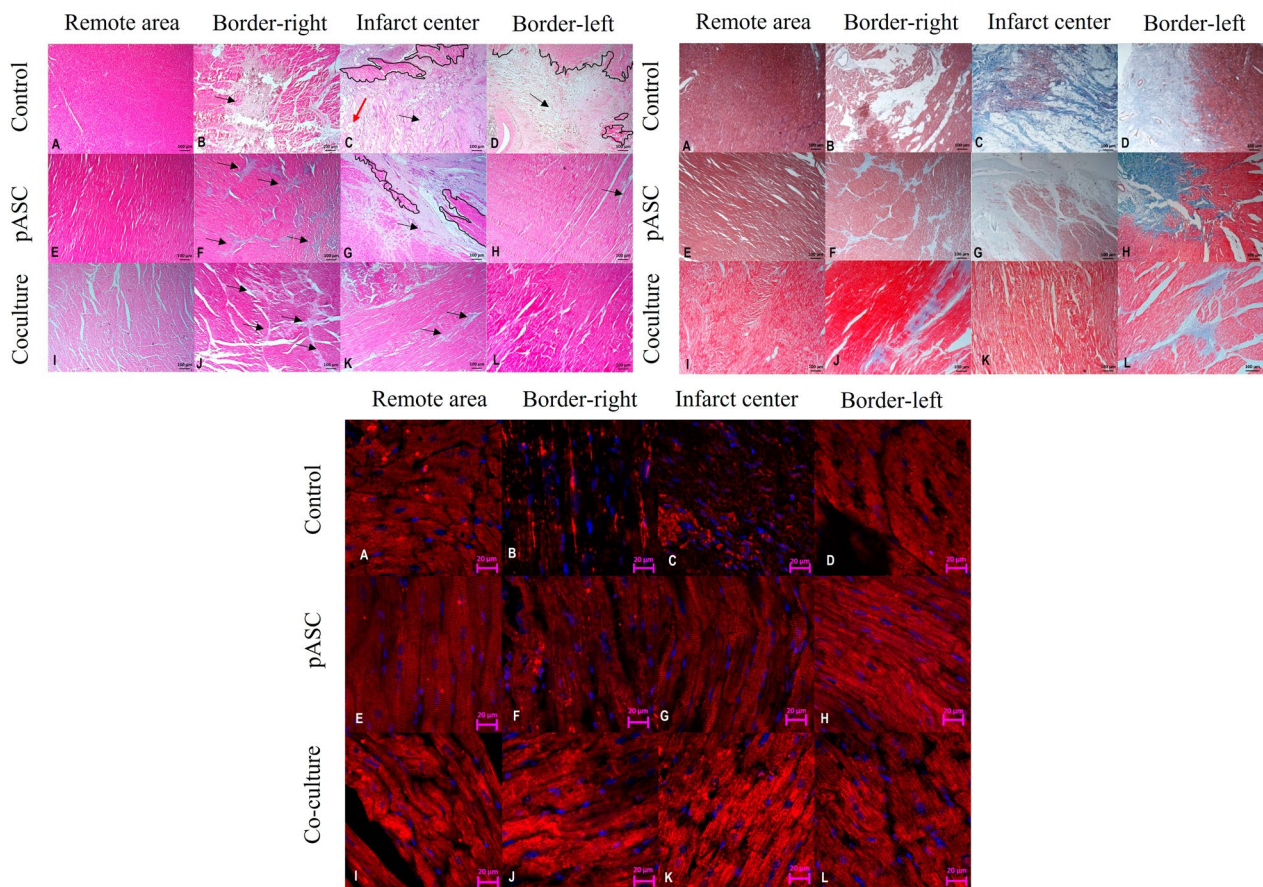


Fig. 4 Histological analysis of porcine myocardium. Representative histological sections of porcine myocardial tissue stained with Hematoxylin and Eosin (H&E) (top left), Masson's Trichrome (top right), and immunofluorescence labeling for α -actinin (bottom left). Illustrating myocardial structural changes across experimental groups: **a–d** control group, **e–h** pASC group, and **i–l** coculture group. Each section corresponds to a specific myocardial region: **a, e, i** remote area, **b, f, j** right border zone, **c, g, k** infarct center, and **d, h, l** left border zone. In the H&E-stained sections (top left), black arrows indicate fibrotic scar regions, while red arrows highlight areas of lipomatosis. Viable cardiomyocyte fibers are delineated by black outlines. All images were captured at 100 × magnification for H&E and Masson's Trichrome staining, whereas immunofluorescence images were acquired at 400 × magnification

minimal in both border zones (Fig. 4f–h). The infarcted area from the coculture-group sample exhibited thin and fine scars stretched between muscle fibers in both border zones, while the center zone had nearly no fibrosis (Fig. 4j–l), similar to the remote sections (Fig. 4a, e, i).

Cardiac muscle is normally dominated by collagen-1 (Fig. 5 top left) and collagen-3 (Fig. 5 top right), which are expressed homogeneously throughout the myocardium, as observed in sections of the remote area in all groups (in all figures labelled as a, e, i). However, in the control group, collagen-1 was overexpressed, especially in the central and border zones, which were also hypocellular and had no fibers (Fig. 5b–top left); however, some areas with lipomatosis showed a reduction in collagen-1 expression. In the pASC group, normal morphology was retained, but the tissue in the central zone was slightly pale (Fig. 5g–top left); neither the border zone nor the remote area showed any differences (Fig. 5f, h–top left). In the coculture group, the corresponding sections showed that all of the regions were similar to the remote region (Fig. 5j–l–top left), except for a few collagen-1-positive areas of fibrosis found in the border left zone (Fig. 5j–top left).

In the control group, collagen-3 expression was decreased in both hypocellular border areas (Fig. 5b, d–top right), except fat tissue in the infarct center, which was normally positive for collagen-3 (Fig. 5c–top right). In the pASC group, collagen-3 expression in the central zone was reduced (Fig. 5g–top right); however, collagen-3 expression in the border zones was similar to that in the remote area (Fig. 5f, h–top right). In the coculture group, all zones (Fig. 5j–l–top right) expressed similar levels of collagen-3, except for the center zone, which had scattered fine tissue positive for collagen-3 between healthy fibers (Fig. 5k–top right), which appeared to be similar to the remote sections (Fig. 5a, e, i–top right).

This study also assessed the presence of myofibroblasts/cells positive for α -SMA. In the control group, there were clusters of myofibroblasts in the central and border zones (Fig. 5b–d–bottom left). Areas with massive myofibroblasts distributed across the sections showed fiber configuration loss, especially in all zones (Fig. 5b–d–bottom left). In the pASC (Fig. 5f–h–bottom left) and coculture (Fig. 5j–l–bottom left) groups, streaks of tissue were positive for α -SMA, indicating that the mesothelial cells which are normally dispersed homogeneously across the myocardium.

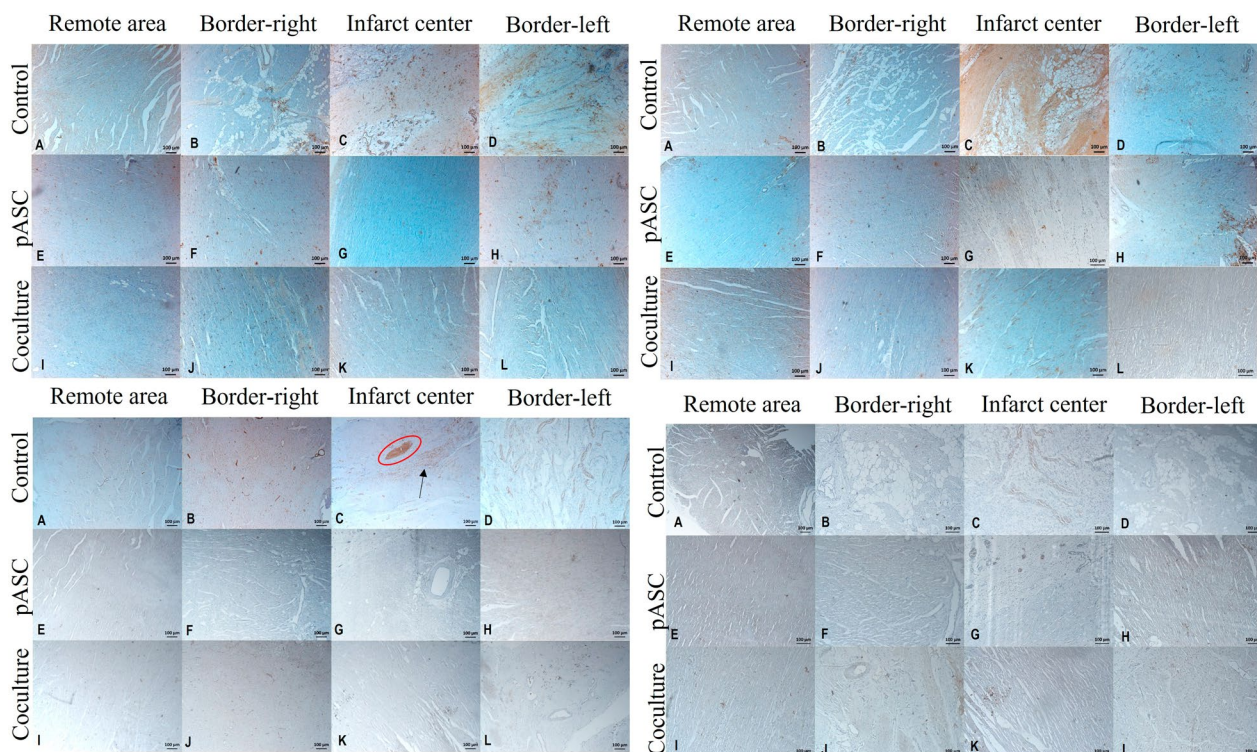


Fig. 5 Immunohistochemical analysis of porcine myocardial sections. Representative immunohistochemical staining of porcine myocardial tissue labeled for Collagen-1 (top left), Collagen-3 (top right), α -SMA (bottom left), and vWF (bottom right). Panels correspond to different experimental groups: **a–d** control, **e–h** pASC, and **i–l** coculture. Each section represents a distinct myocardial region: **a, e, i** remote area, **b, f, j** right border zone, **c, g, k** infarct center, and **d, h, l** left border zone. All images were captured at 100 \times magnification

Blood vessel endothelial cells labelled with vWF were found to be homogeneously distributed across the sections in the coculture group (Fig. 5i, k, l-bottom right). A larger vasculature was clearly observed in the infarct center in the control group (Fig. 5c-bottom right); however, the vasculature was also surrounded by a loosened matrix filler pattern was lost, with muscle fibers being replaced by adipose tissue and showing no vWF expression (Fig. 5b, d-bottom right). The appearance of the pASC (Fig. 5e–h-bottom right) and the coculture group (Fig. 5i–l-bottom right) showed no difference compared to their remote area (Fig. 5a, e, i-bottom right). In the pASC group, fibers shaped positive to vWF stretching along the section might indicate the presence of microvasculature that are abundant across the myocardium, except for center of the infarct; the center region exhibited broken fibers and a larger vWF-positive area (Fig. 5g-bottom right). The pASC group showed homogeneous streaky staining across the sections, indicating the presence of microcapillaries distributed throughout the myocardium. The infarct area in the pASC and coculture groups positive for vWF was tubular in shape with a loosened tissue, and nuclei were arranged in a lattice.

Immunofluorescence labelling of α -actinin in the remote area (Fig. 4a, e, i-bottom) revealed the presence of sarcomeric bands with Z lines organized in a lattice formation. This was not observed in the center (Fig. 4c-bottom) or border zones (Fig. 4b-bottom) in the control group, and the nuclei were found in irregular shapes, sizes and places, while in many areas of the border zone were still retained (Fig. 4d-bottom). The pASC group showed interrupted sarcomeres in the left border zone (Fig. 4f-bottom) but were intact in the central and right border zones (Fig. 4g, h-bottom). The coculture group had sarcomeric bands in all zones (Fig. 4j–l-bottom), and these bands exhibited a similar appearance to those in the remote area (Fig. 4i-bottom).

Cardiomyogenesis activity analysis using real-time qPCR

Cardiomyogenesis activities are indicated by the expression of cTnT, Nkx2.5 and MHC genes. The effect of cell-heart patch treatments on AMI had increased cardiomyogenesis genes significantly, such as cTnT (Fig. 6a), Nkx2.5 (Fig. 6b), and MHC (Fig. 6c) compared to the control ($p < 0.0006$, $p < 0.0001$, and $p = 0.0005$, respectively). The cTnT expression was significantly higher in the pASC ($p = 0.029$) and coculture group ($p = 0.0003$) in the control group, whilst the co-culture had no difference with the pASC group ($p = 0.07$). The Nkx2.5 expression had increased significantly due to the treatment ($p < 0.0001$) while using both pASC or coculture had increased by nearly four-fold compared

to the control group ($p < 0.0001$). However, the Nkx2.5 expression in pASC had no difference with the co-culture group ($p > 0.05$). MHC expression was also increased significantly by the treatment ($p < 0.0001$); the coculture was the highest among the groups. The pASC and the coculture groups had significantly higher compared to the control group ($p = 0.003$ and $p < 0.0001$, respectively), and coculture was significantly higher compared to the pASC group ($p < 0.0001$). Adding both pASC only or coculture in heart patch to the infarct myocardial had significantly increased the progenitor cell expression; cKit ($p = 0.0005$). cKit was found to be significantly higher in the pASC group and the coculture group ($p = 0.0004$ and $p = 0.003$, respectively), while there was no difference between the coculture to the pASC group ($p > 0.05$). Thus, cardiomyogenesis activities appeared to be higher in the co-culture group compared to the pASC group, whilst the control group showed no cardiomyogenesis activities.

The treatments also had significantly lower p21 expression ($p < 0.0001$); the pASC and the coculture groups expressed p21 significantly lower ($p < 0.0001$) compared to the control group, while no difference between the two groups ($p > 0.05$) (Fig. 6e). Interestingly, the p53 expression was significantly higher in the pASC group compared to the control group ($p = 0.0004$), although no difference was seen between the coculture group and the control ($p > 0.05$) (Fig. 6f). The treatment also had significantly decreased Caspase-9 expression; the coculture group expressed Caspase-9 significantly lower than the control group ($p = 0.0007$), the pASC also was significantly lower compared to the control ($p = 0.01$). Caspase-9 expression was statistically not different between the coculture and the pASC groups ($p > 0.05$).

Discussion

This study investigates myocardial regeneration in a pig model of acute myocardial infarction (AMI) using a heart patch derived from an acellular amnion membrane combined with intramyocardial cell injection. Three groups were compared: (1) the coculture group, (2) the porcine amnion stem cell group, and (3) the no-treatment/control group. Infarction modeling was successful in all subjects, with post-ligation serum cardiac troponin T (cTnT) levels increasing 500-fold and creatine kinase (CK) levels rising 50-fold. These biomarkers rapidly enter circulation following myocardial injury, with their serum levels correlating to infarct size [35].

The therapeutic effects of cellular therapy and the heart patch were assessed using clinical and histological data. Electrocardiography (ECG) and echocardiography performed at the study's after 8 weeks post infarction showed no significant abnormalities. Ejection fraction

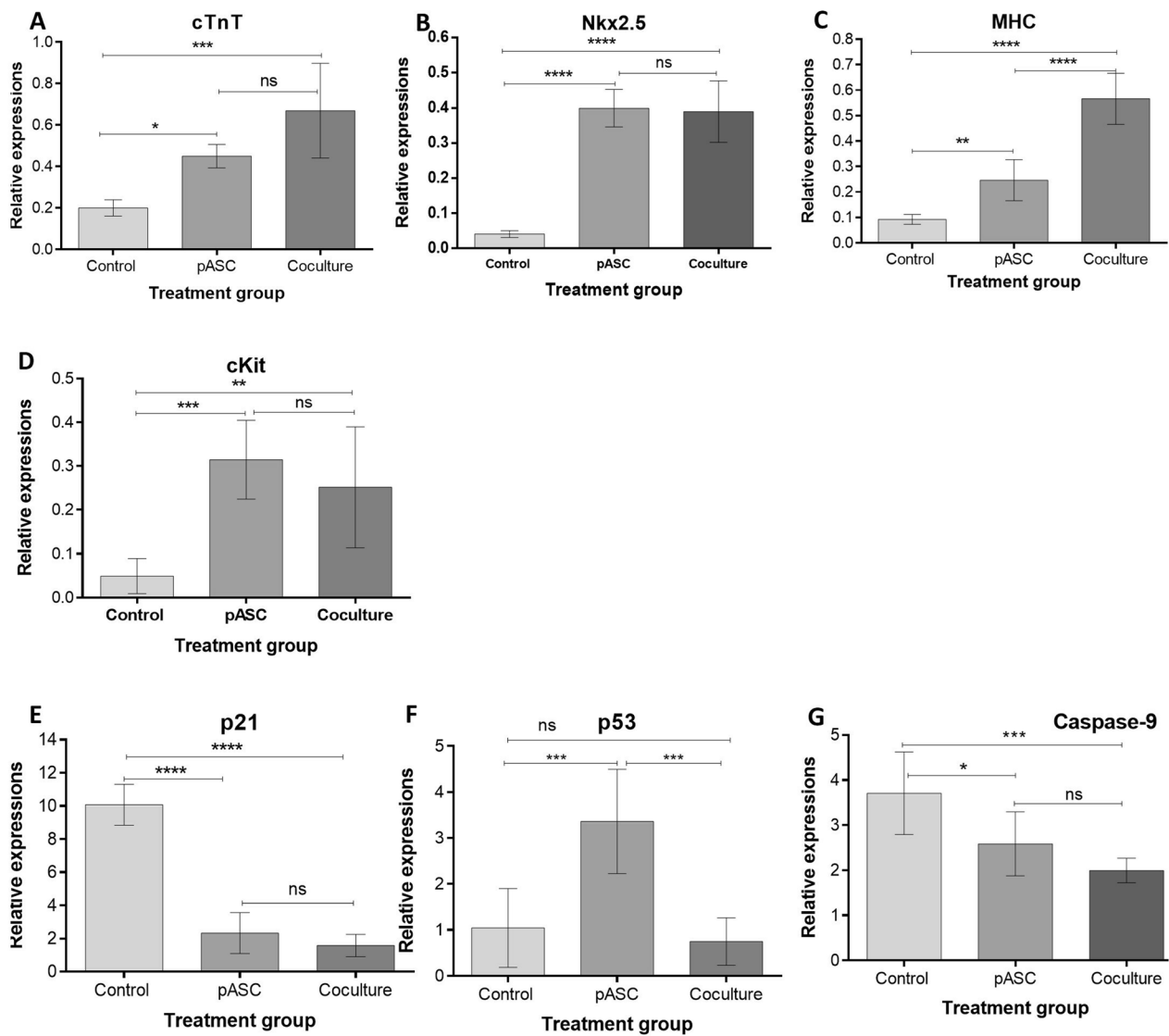


Fig. 6 Gene Expression Analysis of Cardiomyogenesis Markers in a Porcine Myocardial Infarction Model. Quantitative analysis of cardiomyogenesis-related gene expression, including **a** cTnT, **b** Nkx2.5, **c** MHC, **d** cKit, **e** p21, **f** p53, and **g** Caspase-9. Data are presented as mean values (n = 5) with 95% confidence intervals and analyzed using one-way ANOVA, followed by post hoc Tukey’s test to assess group differences. Statistical significance was defined as $p < 0.05$

(EF), left ventricular posterior wall (LVPW) thickness, and interventricular septum (IVS) thickness showed no significant differences among the groups, likely because the posterolateral ventricular (PLV) ligation affected less than 10% of the ventricular wall—insufficient to cause major functional impairment. Additionally, interventions were applied within 60 min post-ligation, during the “golden period,” potentially preserving heart function. Prior studies suggest that cTnT levels exceeding 2.98 µg/L post-infarction predict a decline in EF below 40% within three months [36]. In our model, post-infarction cTnT levels were significantly lower (500 pg/

mL), suggesting minimal myocardial damage. Previous attempts to induce a larger infarction via left anterior descending (LAD) artery ligation resulted in high mortality, with three out of five pigs dying immediately. Histological analysis revealed extensive infarction of the ventricular wall, tricuspid valve, and interventricular septum. Additionally, prolonging anesthesia beyond 60 min increased mortality risk, making delayed heart patch application impractical.

Regional wall motion abnormalities (RWMA) were the only clinical parameter that differed significantly among groups. Infarction disrupted cardiac kinetics, whereas

treatment improved function compared to the control. The co-culture group exhibited the highest regenerative potential, with 60% of subjects showing RWMA improvement, compared to 25% in the pASC group. In contrast, no myocardial regeneration was observed in the control group, where infarcted tissue displayed hypocellular scarring, overexpression of collagen-1, and disrupted sarcomeric bands. RWMA serves as a sensitive indicator of myocardial fiber impairment. A study on RWMA following anterior and inferior infarction found that all myocardial infarctions led to RWMA worsening. In anterior infarctions, impairment progressed from the proximal anterior region toward the distal apical zone, whereas in inferior infarctions, the basal segment of the inferior-posterior wall was affected, with relative preservation toward the apical region, depending on the infarct-related vessel [37]. Furthermore, the extensive hypocellularity observed was attributed to widespread cardiomyocyte death and insufficient endogenous repair, ultimately leading to myocardial dysfunction.

Following ischemia, over one billion cardiomyocytes in the affected region die, triggering an inflammatory response. Necrotic cells release cytokines and damage-associated molecular patterns (DAMPs), inducing inflammation [38], and macrophage recruitment for debris clearance [39]. Apoptotic cardiomyocytes undergo nuclear condensation within two weeks and disappear by four weeks [40].

Classic infarct morphology, such as wavy fibers, necrotic accumulation, or contraction bands [41], was absent due to the study's eight-week post-infarction timeline. The coculture group exhibited preserved sarcomere integrity, with Z-bands arranged in a lattice structure, uniformly sized nuclei, and minimal fibrosis at infarct borders. In contrast, none of the control group subjects exhibited RWMA recovery, as no viable muscle fibers remained to sustain contraction. Interestingly, some control group samples displayed adipose tissue-like structures, indicating lipomatous metaplasia in myocardial infarction (LMMI). LMMI occurs when fibrotic myocardial scars undergo adipose transformation due to myofibroblast differentiation in response to scarring and poor vascularization [42]. This suggests that PLV ligation in our study induced severe myocardial destruction. Progressive myofibrillar degeneration leads to lipid accumulation [43, 44], and increased mortality due to ventricular tachycardia [45]. Masson's trichrome staining confirmed extensive fibrosis in the control group, with dense collagen deposits in infarct zones [46]. Areas of lipid accumulation tested positive for collagen-3, confirming the presence of mature adipose tissue [47, 48]. Control group scars appeared hypocellular, disorganized, and extensively transformed into adipose tissue.

In our study, both coculture and pASC-treated groups exhibited significantly reduced myocardial scar formation across all infarcted zones compared to the control group, alongside upregulated expression of cardiomyogenesis-associated genes. The transplantation of pASCs into the infarcted myocardium in both intervention groups likely attenuated post-infarction inflammation by counteracting excessive reactive oxygen species (ROS) accumulation. Ischemic injury precipitates ROS overproduction, leading to mitochondrial dysfunction, NAD⁺ depletion, intracellular calcium dysregulation, and the activation of proteolytic enzymes, including matrix metalloproteinases (MMPs) [49]. Specifically, MMP-1, secreted by macrophages and myofibroblasts, induces collagen degradation in the extracellular matrix (ECM), contributing to structural disarray and myocardial fibrosis [50]. Moreover, MMPs facilitate the proteolysis of key cytoskeletal proteins, such as α -actinin, within cardiomyocytes [51, 52], further exacerbating ECM fragmentation and fibrotic remodeling. Histopathological analysis of the control group revealed pronounced sarcomeric disruption, characterized by vacuolated, rod-shaped myofibers and a marked reduction in α -actinin puncta, indicative of severe infarction [53]. Notably, these degenerative features were absent in both treatment groups, suggesting a protective effect conferred by pASC and coculture transplantation.

Amniotic-derived stem cells have been reported to exert potent immunomodulatory effects by suppressing proinflammatory cytokine release [54]. Specifically, they facilitate the transition of proinflammatory Th1 and Th17 cells into reparative Th2 phenotypes, while promoting M1-to-M2 macrophage polarization, thereby enhancing tissue regeneration [55]. Similar immunoregulatory effects were demonstrated in prior studies, wherein amniotic epithelial cell (AEC) transplantation facilitated complete corneal repair following alkaline-induced injury in rabbits [56]. Importantly, the pASCs employed in this study lacked expression of HLA-DR and HLA-ABC, potentially enabling immune evasion and preventing allogeneic rejection [57].

Histological analysis further revealed sparse collagen-3 expression within the infarct border zone of the pASC group and within the infarct core of the coculture group. AECs have been shown to suppress fibrosis and regulate collagen synthesis [58], consistent with findings in rodent models demonstrating persistent collagen-3 expression in myocardial regions extending beyond 1 cm from the primary infarct zone [59]. Notably, in the coculture group, certain regions of the infarct border exhibited a predominance of collagen-3 over collagen-1. Given that collagen-3 contributes to myocardial compliance and facilitates tissue remodeling, whereas collagen-1

provides tensile strength and resists contraction, this differential expression may facilitate biomechanical adaptation during myocardial repair. The presence of fine, nucleated collagen-3 fibers suggests the activation of cardiofibroblasts, potentially contributing to cardiomyogenesis.

Although the pASC group demonstrated regions of reduced scar formation, myocardial regeneration was more pronounced in the coculture group. Previous studies have demonstrated that collagen-3 expression enhances cellular proliferation, migration, angiogenesis, and upregulation of α -actinin and connexin-43 (CX43), all of which are critical for myocardial repair [60]. Both the pASC and coculture groups exhibited no significant differences in collagen-1 expression between the infarcted and remote myocardial regions. In contrast, the control group displayed extensive collagen degradation and disorganization, impairing myocardial contractility. Progressive myocardial fibrosis disrupts electrical conduction, predisposing affected regions to ectopic focal activity and reentrant arrhythmias, thereby increasing the risk of heart failure [61]. As infarcted myocardium loses mechanical integrity, compensatory hypertrophic remodeling in adjacent healthy myocardium induces excessive strain, triggering further collagen deposition and crosslinking, ultimately leading to myocardial stiffening, impaired ventricular compliance, and reduced cardiac output [8]. After eight weeks of observation, the control group exhibited extensive fibrosis within both infarct border regions. In contrast, our previous study employing a one-month infarction model demonstrated comparatively less severe fibrotic remodeling at the infarct periphery [62], suggesting that prolonged mechanical strain exacerbates collagen denaturation over time. Chronic collagen degradation is a hallmark of heart failure progression [63] and often precedes the complete removal of necrotic cardiomyocytes [64].

The superior regenerative outcomes observed in the coculture group after eight weeks of treatment may not be solely attributable to the presence of amniotic stem cells. Cardiomyocytes possess intrinsic antioxidant defense mechanisms to mitigate ROS-induced damage following infarction. Specifically, cardiomyocytes express dimethylarginine dimethyl-aminohydrolase (DDAH), which neutralizes intracellular ROS and suppresses apoptosis via the superoxide dismutase 2 (SOD2)-dependent pathway [65]. The coculture group exhibited finer scar architecture and improved myocardial function, whereas the pASC group displayed broader scar formation, suggesting that pASCs alone may be insufficient to counteract the severe oxidative stress associated with acute myocardial infarction. [49]. The survival and reparative potential of transplanted

stem cells are likely compromised under conditions of heightened inflammation, particularly in the presence of excessive ROS and proinflammatory cytokines such as TNF- α , IL-1 β , and IL-6, which are secreted by activated macrophages in response to myocardial injury [66].

Furthermore, this study employed heterogeneous primary cardiac cell populations, encompassing multiple cellular constituents beyond cardiomyocytes. Notably, cardiomyocytes express Notch1, a key regulator of cardiac progenitor cell differentiation, apoptosis inhibition, and neovascularization [67]. Endothelial cells, which comprise a substantial fraction of the cardiac cellular milieu ($63.3 \pm 5.4\%$) compared to non-endothelial cell populations ($29.9 \pm 5.9\%$) [68], also play a pivotal role in myocardial regeneration. Endothelial cells within the endocardium and microvascular networks secrete neuregulin-1 (NRG-1), a growth factor that enhances cardiomyocyte survival, promotes myocardial regeneration, augments angiogenesis, and facilitates cellular and vesicular transport within the infarct region [69].

Following myocardial injury, a substantial transformation of cardiac fibroblasts into myofibroblasts occurs after the clearance of necrotic cellular debris, a process mediated by interleukin-1 (IL-1) signaling [70]. The presence of myofibroblasts is marked by α -smooth muscle actin (α -SMA) expression, which is also associated with mesodermal layers within the capillary walls [71]. Our study demonstrated a significantly higher prevalence of myofibroblasts in the control group at eight weeks post-infarction. Prior research has reported that myofibroblast populations increase up to 20-fold within days following infarction, with densities reaching several thousand cells per mm^2 and persisting for several weeks [72]. Conversely, the pASC and coculture groups exhibited a markedly reduced myofibroblast presence, suggesting that these cell-based interventions attenuate fibroblast-to-myofibroblast differentiation.

The pASC and coculture therapies were delivered through a three-dimensional (3D) acellular heart patch, which enhanced cellular retention within the infarcted myocardium while subjecting the transplanted cells to continuous biomechanical stimulation. This mechanical environment played a critical role in directing cardiomyogenesis. Myocardial contraction and relaxation rely on the intricate arrangement of extracellular matrix (ECM) fibers, which facilitate the transmission of biomechanical forces in a synchronized manner. Cardiofibroblasts positioned between ECM fibers are hypothesized to regulate myofibroblast differentiation by modulating focal adhesion kinase (FAK) signaling, thereby preventing excessive collagen deposition while maintaining ECM homeostasis [73]. Notably, these

regulatory mechanisms were absent in traditional two-dimensional (2D) culture systems. The biomechanical properties of the heart patch likely contributed to myocardial repair by reinforcing the infarcted ventricular wall. With an ultimate tensile strength (ϵ UTS) of approximately 5.48 ± 1.96 MPa and a collagen stiffness modulus of 308.13 ± 60.28 MPa [74], the patch functioned as a mechanical scaffold, mitigating infarct expansion and preventing ventricular wall thinning. Previous studies have demonstrated that biomechanical stimulation facilitates stem cell differentiation into functionally mature cardiomyocytes, promoting the formation of native-like myocardial tissue [75].

Histological analysis revealed significant heterogeneity in vascularization across different infarct regions. In severely fibrotic and hypocellular regions, α -SMA-positive cells exhibited a rounded morphology and a lack of vWF expression, indicating an absence of functional vasculature. In contrast, infarcted regions with extensive cellular infiltration displayed α -SMA- and vWF-positive cells with a larger, rounded morphology, suggesting ongoing neovascularization and tissue remodeling. The presence of functional vasculature in these regions may facilitate myocardial repair, whereas compact, avascular scar tissue likely represents terminal fibrosis. Angiogenesis, the formation of new blood vessels from preexisting vasculature, is a critical component of post-infarction tissue repair. This process is driven by proangiogenic mediators such as thrombin, fibrinogen, and thymosin β -4, secreted by activated platelets and inflammatory cells in response to ischemic injury [76]. Studies have demonstrated that adipose-derived stem cells (ASCs) enhance post-infarction cardiac function by secreting proangiogenic factors such as vascular endothelial growth factor (VEGF), transforming growth factor-beta 1 (TGF- β 1), and interleukin-8 (IL-8), thereby promoting neovascularization and myocardial regeneration [77, 78].

To investigate the molecular mechanisms underlying myocardial regeneration, we analyzed the expression of key cardiomyogenic genes, including markers of cardiomyocyte differentiation (cardiac troponin T [cTnT], myosin heavy chain [MHC], and Nkx2.5), progenitor cell markers (c-Kit), and apoptosis-related genes (p21, p53, and caspase-9). cTnT is a fundamental driver of cardiomyogenesis, playing a pivotal role in sarcomere assembly and myocardial contractility [79]. In our study, cTnT expression was significantly upregulated in the coculture group, consistent with increased MHC expression, indicative of enhanced cardiomyocyte differentiation and functional integration. Prior research has reported significantly lower MHC expression in failing human hearts (2.2

$\pm 3.5\%$) compared to normal hearts ($33.3 \pm 18.9\%$) [80]. Notably, our findings demonstrated that the coculture group exhibited the highest MHC expression among all experimental groups, further supporting its therapeutic potential.

c-Kit expression was also significantly elevated in both the pASC and coculture groups compared to the control group. Given that pASCs primarily consist of progenitor cells, this observation suggests that coculture therapy facilitates the differentiation of pASCs into cardiomyocytes. c-Kit functions as a tyrosine kinase receptor involved in hematopoiesis, stem cell maintenance, and cardiac progenitor cell function [81]. Previous studies have demonstrated that c-Kit activation induces cardiomyocyte proliferation and reverses cellular senescence, thereby promoting myocardial repair [82]. The Phase III PERFECT trial, which involved the intramyocardial injection of c-Kit+/CD117+/CD133+/CD34+ hematopoietic stem cells during coronary artery bypass grafting (CABG), reported a 60% improvement in cardiac function in acute myocardial infarction (AMI) patients [83].

Nkx2.5, a critical transcription factor in cardiac development, was significantly upregulated in both the pASC and coculture groups, exhibiting a four-fold increase compared to the control group. Nkx2.5 is essential for myocardial repair, regulating the transcription of α -actinin and β -MHC to facilitate sarcomeric organization and functional integration of newly differentiated cardiomyocytes [84]. Mutations in Nkx2.5 have been linked to congenital heart defects, arrhythmias, and impaired myocardial differentiation [85]. Interestingly, p53 expression was highest in the pASC group, reaching levels four-fold greater than those observed in normal, non-infarcted myocardium. In contrast, the coculture group exhibited the lowest p53 expression. Given that oxidative stress induces DNA damage and apoptosis in infarcted myocardium, it is plausible that elevated p53 expression in the pASC group was a response to reactive oxygen species (ROS)-induced cellular damage, leading to selective apoptosis of compromised pASCs. p53 is known to regulate stem cell differentiation and serves as a tumor suppressor by modulating the cell cycle, preventing unchecked proliferation, and maintaining genomic integrity [86].

p53 also activates p21, a cyclin-dependent kinase inhibitor that orchestrates cell cycle arrest and transcriptional regulation. p21 plays a dual role in apoptosis, either promoting cell survival or facilitating programmed cell death under oncogenic stress [33]. Dysregulation of p21 has been implicated in tumorigenesis, with phosphorylation at Ser-146 inactivating the ROCK/LIMK/cofilin pathway and

promoting invasive cellular behavior via PI3 K and MEK signaling [87].

In our study, p21 expression in both intervention groups was approximately one-fold lower than in normal myocardium, closely resembling levels observed in healthy hearts. Conversely, the control group exhibited p21 expression levels ten times higher than those in normal myocardium, likely due to extensive apoptosis and DNA damage. The addition of amniotic stem cells may have mitigated this effect by reducing proinflammatory cytokines such as TNF- α , IL-6, IL-10, and COX-2 [54]. Caspase-9 expression was highest in the control group, consistent with its role in apoptosis regulation via the cysteine protease pathway, which can lead to irreversible cardiomyocyte damage [88]. While Caspase-9 is typically upregulated during post-infarction healing to reduce apoptosis and prevent myocardial fusion [89, 90], its expression did not significantly differ among the intervention groups. This suggests a distinct apoptotic mechanism in the control group compared to the intervention groups.

Histological analysis of the control group revealed extensive hypocellular and acellular regions within mature scar tissue, yet apoptosis levels remained high even at eight weeks post-infarction. This suggests ongoing cell death in the remaining viable tissue surrounding the infarct. One possible explanation is that mechanical stress overload in the infarct border zone triggered secondary infarctions, leading to excessive reactive oxygen species (ROS) production and further cell loss [91]. Future studies should assess ROS levels and cytokine profiles beyond eight weeks post-intervention, particularly in the infarct border zone.

The addition of cardiac cells to pASCs may have enhanced cardiomyogenesis while reducing cellular stress, thereby eliminating the need for cell cycle arrest. This is supported by the significantly lower expression of p53 and p21 in the coculture group. Further investigation is needed to determine whether this group had a reduced risk of mutation due to DNA damage.

Similarly, 3D biomatrices, such as viable amniotic membranes in rat models, have been shown to significantly improve LV wall thickness within seven days of application and reduce left atrial diameter for up to 90 days ($p < 0.05$) [18]. Another clinical study involving 24 patients with non-ischemic dilated cardiomyopathy utilized autologous CD56-positive skeletal muscle cell-layer patches, cultured in poly-N-isopropylacrylamide and fibrin glue, contained 6.0×10^7 cells, with up to five or six patches covering the anterior and lateral left ventricular (LV) walls. enhanced exercise capacity and cardiac function with a 5-year survival rate of 90.9% after a mean follow-up of 47.5 ± 4.3 months [16].

The primary limitation of this study was the inability to ensure the survival of pigs after inducing a sufficiently extensive infarct area to cause significant cardiac dysfunction. Future research should prioritize the development of models capable of generating larger infarct regions, such as through ligation of the first or second diagonal branch to induce anterior infarction. Additionally, further investigations should examine the effects of interventions on chronic infarcts while advancing translational applications for human cardiac repair.

Conclusion

This study demonstrates the superior regenerative potential of coculture therapy in myocardial repair compared to pASC transplantation alone. The significant improvements observed in scar architecture, extracellular matrix remodeling, and cardiac function in the coculture group underscore the therapeutic advantage of integrating heterogeneous primary cardiac cells into stem cell-based interventions. These findings suggest that coculture strategies may optimize cellular interactions, enhance cardiomyogenesis, and improve functional recovery post-infarction..

Supplementary Information

The online version contains supplementary material available at <https://doi.org/10.1186/s13019-025-03453-3>.

Additional file 1

Additional file 2

Additional file 3

Acknowledgements

The authors would like to thank all members of the veterinarian team of Rumah Sakit Hewan Pendidikan Sekolah Kedokteran Hewan dan Biomedis IPB University for their assistance throughout all surgeries performed to induce myocardial infarction.

Author contributions

MAP: conceptualization, investigation, methodology, funding acquisition, resources, writing—review and editing; NS: conceptualization, formal analysis, investigation, methodology, resources, validation, writing—original draft; TWS: conceptualization, investigation, writing—review and editing; TRK: data curation, investigation, project administration, validation, writing—review and editing; NAF: data curation, investigation, writing—review and editing; BK: data curation, investigation, writing—review and editing; DN: formal analysis, investigation, methodology, resources, writing—review and editing; G: formal analysis, investigation, methodology, resources, writing—review and editing; PWB: conceptualization, methodology, supervision, writing—review and editing; S: conceptualization, methodology, supervision, writing—review and editing; IA: conceptualization, methodology, resources, supervision, writing—review and editing.

Funding

This study was partially funded by the Indonesian National Research and Innovation Agency under Grant No. 008/E4/AK.04.PRN/2021.

Data availability

No datasets were generated or analysed during the current study.

Declarations**Ethics approval**

All protocols performed in this study complied with the guidelines regarding the use of animals in research outlined in the Declaration of Helsinki and were reviewed and approved by the local Animal Experimentation Unit Ethical Committee of the Institut Pertanian Bogor, Indonesia (Number 158/KEH/SKE/XII/2019). All protocols for human amnion collection performed in this study have been reviewed and approved by the Ethics Committee of Faculty of Medicine, University of Indonesia (Number KET-1307/UN2.F1/ETIK/PPM.00.02/2019).

Consent for publication

Not applicable.

Conflict of interest

The authors declare no competing interests.

Author details

¹Division of Thoracic, Cardiac and Vascular Surgery, Department of Surgery, Faculty of Medicine, Universitas Indonesia, Jakarta 10430, Indonesia. ²Indonesian Medical Education and Research Institute, Universitas Indonesia, Jakarta 10430, Indonesia. ³Division of Adult Cardiac Surgery, Harapan Kita National Cardiovascular Center, Jakarta 11420, Indonesia. ⁴Division of Surgery and Radiology, School of Veterinary Medicine and Biomedical Sciences, IPB University, Bogor 16680, Indonesia. ⁵Division of Pediatric and Congenital Cardiac Surgery, Harapan Kita National Cardiovascular Center, Jakarta 11420, Indonesia. ⁶Division of Cardiothoracic Surgery, Department of Surgery, Faculty of Medicine, Universitas Gadjah Mada, Yogyakarta 55284, Indonesia. ⁷Division of Cardiology, Department of Internal Medicine, Faculty of Medicine, Universitas Indonesia, Jakarta 10430, Indonesia.

Received: 24 October 2024 Accepted: 6 April 2025

Published online: 09 May 2025

References

- Benjamin EJ, Blaha MJ, Chiuve SE, Cushman M, Das SR, Deo R, Ferranti SDD, Floyd J, Fornage M, Gillespie C, Isasi CR, Jiménez MC, Jordan LC, Judd SE, Lackland D, Lichtman JH, Lisabeth L, Liu S, Longenecker CT, Mackey RH, Matsushita K, Mozaffarian D, Mussolino ME, Nasir K, Neumar RW, Palaniappan L, Pandey DK, Thiagarajan RR, Reeves MJ, Ritchey M, Rodriguez CJ, Roth GA, Rosamond WD, Sasson C, Towfighi A, Tsao CW, Turner MB, Virani SS, Voeks JH, Willey JZ, Wilkins JT, Wu JH, Alger HM, Wong SS, Muntner P. Heart disease and stroke statistics—2017 update: a report from the American Heart Association. *Circulation*. 2017;135:e146–603.
- Tarmizi SN. Cegah Penyakit Jantung dengan Menerapkan Perilaku CERDIK dan PATUH. In: Ministry H (ed). Kemenkes, Jakarta. 2023
- HUMAS. 2018. Peserta JKN-KIS Semarangkan Senam Sehat Kolosal [Online]. Available: <https://bpjs-kesehatan.go.id/bpjs/index.php/post/read/2018/855/18818-Participants-of-JKN-KIS-Increase-Colossal-Healthy-Gymnastics>. Accessed
- Usman Y, Iriawan R, Rosita T, Lusiana M, Kosen S, Kelly M, Forsyth S, Rao C. Indonesia's sample registration system in 2018: a work in progress. *J Popul Soc Stud*. 2018;27:39–52.
- Gajanana D, Shah M, Junpapart P, Romero-Corral A, Figueredo VM, Bozorgnia B. Mortality in systolic heart failure revisited: Ischemic versus non-ischemic cardiomyopathy. *Int J Cardiol*. 2016;224:15–7.
- Gombozhapova A, Rogovskaya Y, Shurupov V, Rebenkova M, Kzhyshkowska J, Popov SV, Karpov RS, Ryabov V. Macrophage activation and polarization in post-infarction cardiac remodeling. *J Biomed Sci*. 2017;24:1–11.
- Richardson WJ, Clarke SA, Quinn TA, Holmes JW. Physiological implications of myocardial scar structure. *Compr Physiol*. 2015;5:1877–909.
- Gombozhapova A, Rogovskaya Y, Shurupov V, Rebenkova M, Kzhyshkowska J, Popov SV, Karpov RS, Ryabov V. Macrophage activation and polarization in post-infarction cardiac remodeling. *J Biomed Sci*. 2017;24:13.
- Elgendy IY, Mahtta D, Pepine CJ. Medical therapy for heart failure caused by ischemic heart disease. *Circ Res*. 2019;124(11):1520–35. <https://doi.org/10.1161/CIRCRESAHA.118.313568>.
- Eschenhagen T, Bolli R, Braun T, Field LJ, Fleischmann BK, Frisen J, Giacca M, Hare JM, Houser S, Lee RT, Marban E, Martin JF, Molkentin JD, Murry CE, Riley PR, Ruiz-Lozano P, Sadek HA, Sussman MA, Hill JA. Cardiomyocyte regeneration: a consensus statement. *Circulation*. 2017;136:680–6.
- Bergmann O, Bhardwaj RD, Bernard S, Zdunek S, Barnabé-Heider F, Walsh S, Zupicich J, Alkass K, Buchholz BA, Druid H. Evidence for cardiomyocyte renewal in humans. *Science*. 2009;324:98–102.
- Jones NR, Roalfe AK, Adoki I, Richard Hobbs FD, Taylor CJ. Survival of patients with chronic heart failure in the community: a systematic review and meta-analysis protocol. *Syst Rev*. 2018;7:151.
- Kobashigawa J, Khush K, Colvin M, Acker M, Van-Bakel A, Eisen H, Naka Y, Patel J, Baran DA, Daun T, Luu M, Olymbios M, Rogers J, Jeevanandam V, Esmailian F, Pagani FD, Lima B, Stehlik J. Report from the American Society of transplantation conference on donor heart selection in adult cardiac transplantation in the United States. *Am J Transpl*. 2017;17:2559–66.
- Severino P, Mather PJ, Pucci M, D'Amato A, Mariani MV, Infusino F, Birtolo LI, Maestrini V, Mancone M, Fedele F. Advanced heart failure and end-stage heart failure: does a difference exist. *Diagnostics*. 2019;9:170.
- Bolognese L, Neskovic AN, Parodi G, Cerisano G, Buonamici P, Santoro GM, Antoniucci D. Left ventricular remodeling after primary coronary angioplasty. *Circulation*. 2002;106:2351–7.
- Domae K, Miyagawa S, Yoshikawa Y, Fukushima S, Hata H, Saito S, Kainuma S, Kashiyama N, Iseoka H, Ito E, Harada A, Takeda M, Sakata Y, Toda K, Pak K, Yamada T, Sawa Y. Clinical outcomes of autologous stem cell-patch implantation for patients with heart failure with nonischemic dilated cardiomyopathy. *J Am Heart Assoc*. 2021;10:e008649.
- Lang CI, Dahmen A, Vasudevan P, Lemcke H, Gabel R, Öner A, Ince H, David R, Wolfen M. Cardiac cell therapies for the treatment of acute myocardial infarction in mice: systematic review and meta-analysis. *Cytotherapy*. 2023;25:640–52.
- Cargnoni A, di Marcello M, Campagnoli M, Nassuato C, Albertini A, Parolini O. Amniotic membrane patching promotes ischemic rat heart repair. *Cell Transpl*. 2009;18:1147–59.
- Bakhshandeh B, Sorboni SG, Ranjbar N, Deyhimfar R, Abtahi MS, Izady M, Kazemi N, Noori A, Pennisi CP. Mechanotransduction in tissue engineering: Insights into the interaction of stem cells with biomechanical cues. *Exp Cell Res*. 2023;431:113766.
- Raposo L, Lourenço AP, Nascimento DS, Cerqueira R, Cardim N, Leite-Moreira A. Human umbilical cord tissue-derived mesenchymal stromal cells as adjuvant therapy for myocardial infarction: a review of current evidence focusing on pre-clinical large animal models and early human trials. *Cytotherapy*. 2021;23:974–9.
- Konertz W, Angeli E, Tarasnov G, Christ T, Kroll J, Dohmen PM, Krogmann O, Franzbach B, Pace Napoleone C, Gargiulo G. Right ventricular outflow tract reconstruction with decellularized porcine xenografts in patients with congenital heart disease. *J Heart Valve Dis*. 2011;20:341.
- Putra MA, Sandora N, Suwanti, Nurhayati RW, Nauli R, Kusuma TR, Fitria NA, Ardiansyah, Muttaqin C, Makdinata W, Alwi I. Transport viable heart tissue at physiological temperature yielded higher human cardiomyocytes compared to the conventional temperature. *Cell Tissue Bank*. 2022;23:717–27.
- Sandora N, Putra MA, Nurhayati RW, Suwanti, Nauli R, Kusuma TR, Fitria NA, Ardiansyah, Muttaqin C, Makdinata W. Characterisation of the single-cell human cardiomyocytes taken from the excess heart tissue of the right ventricular outlet in congenital heart disease. *Cell Tissue Bank*. 2021;23(3):489–97.
- Newman PJ, Newman DK. Signal transduction pathways mediated by PECAM-1: new roles for an old molecule in platelet and vascular cell biology. *Arterioscler Thromb Vasc Biol*. 2003;23:953–64.
- Pontén A, Walsh S, Malan D, Xian X, Schéele S, Tarnawski L, Fleischmann BK, Jovinge S. FACS-based isolation, propagation and characterization

- of mouse embryonic cardiomyocytes based on VCAM-1 surface marker expression. *PLoS ONE*. 2013;8: e82403.
26. Sandora N, Putra MA, Nurhayati RW, Nauli R, Kusuma TR, Fitri NA, Muttaqin C, Makdinata W, Alwi I. Characterisation of the single-cell human cardiomyocytes taken from the excess heart tissue of the right ventricular outlet in congenital heart disease. *Cell Tissue Bank*. 2021;23:489–97.
 27. Iranpour S, Mahdavi-Shahri N, Miri R, Hasanzadeh H, Bidkhorri HR, Naderi-Meshkin H, Zahabi E, Matin MM. Supportive properties of basement membrane layer of human amniotic membrane enable development of tissue engineering applications. *Cell Tissue Bank*. 2018;19:357–71.
 28. (AVMA), AVMA. American Veterinary Medical Association (AVMA) Guidelines for the Euthanasia of Animals: 2020 Edition. Illinois; 2020
 29. Nagao M, Hamilton JL, Kc R, Berendsen AD, Duan X, Cheong CW, Li X, Im H-J, Olsen BR. Vascular Endothelial Growth Factor in Cartilage Development and Osteoarthritis. *Sci Rep*. 2017;7:13027.
 30. Tiso N, Majetti M, Stanchi F, Rampazzo A, Zimbello R, Nava A, Danieli G. Fine mapping and genomic structure of ACTN2, the human gene coding for the sarcomeric isoform of α -Actinin-2, expressed in skeletal and cardiac muscle. *Biochem Biophys Res Commun*. 1999;265:256–9.
 31. Collinson PO, Boa FG, Gaze DC. Measurement of cardiac troponins. *Ann Clin Biochem*. 2001;38:423–49.
 32. Markmee R, Aungsuchawan S, Tancharoen W, Narakornsak S, Pothacharoen P. Differentiation of cardiomyocyte-like cells from human amniotic fluid mesenchymal stem cells by combined induction with human platelet lysate and 5-azacytidine. *Heliyon*. 2020;6: e04844.
 33. Macleod KF, Sherry N, Hannon G, Beach D, Tokino T, Kinzler K, Vogelstein B, Jacks T. p53-dependent and independent expression of p21 during cell growth, differentiation, and DNA damage. *Genes Dev*. 1995;9:935–44.
 34. Waldman T, Kinzler KW, Vogelstein B. p21 is necessary for the p53-mediated G1 arrest in human cancer cells. *Can Res*. 1995;55:5187–90.
 35. Wagner I, Mair J, Fridrich L, Artner-Dworzak E, Lechleitner P, Morass B, Dienstl F, Puschendorf B. Cardiac troponin T release in acute myocardial infarction is associated with scintigraphic estimates of myocardial scar. *Coron Artery Dis*. 1993;4:537–44.
 36. Panteghini M, Cuccia C, Bonetti G, Giubbini R, Pagani F, Bonini E. Single-point cardiac troponin T at coronary care unit discharge after myocardial infarction correlates with infarct size and ejection fraction. *Clin Chem*. 2002;48:1432–6.
 37. Feldmann KJ, Goldstein JA, Marinescu V, Dixon SR, Raff GL. Disparate impact of ischemic injury on regional wall dysfunction in acute anterior vs inferior myocardial infarction. *Cardiovasc Revasc Med*. 2019;20:965–72.
 38. Briceno N, Schuster A, Lumley M, Perera D. Ischaemic cardiomyopathy: pathophysiology, assessment and the role of revascularisation. *Heart*. 2016;102:397–406.
 39. Cattin A-L, Burden JJ, van Emmenis L, Mackenzie FE, Hoving JJ, Calavia NG, Guo Y, McLaughlin M, Rosenberg LH, Quereda V. Macrophage-induced blood vessels guide Schwann cell-mediated regeneration of peripheral nerves. *Cell*. 2015;162:1127–39.
 40. Takemura G, Ohno M, Hayakawa Y, Misao J, Kanoh M, Ohno A, Uno Y, Minatoguchi S, Fujiwara T, Fujiwara H. Role of apoptosis in the disappearance of infiltrated and proliferated interstitial cells after myocardial infarction. *Circ Res*. 1998;82:1130–8.
 41. Bouchardy B, Majno G. Histopathology of early myocardial infarcts: a new approach. *Am J Pathol*. 1974;74:301.
 42. Su L, Siegel JE, Fishbein MC. Adipose tissue in myocardial infarction. *Cardiovasc Pathol*. 2004;13:98–102.
 43. Borisov AB, Ushakov AV, Zagorulko AK, Novikov NY, Selivanova KF, Edwards CA, Russell MW. Intracardiac lipid accumulation, lipotrophy of muscle cells and expansion of myocardial infarction in type 2 diabetic patients. *Micron*. 2008;39:944–51.
 44. Nucifora G, Aquaro GD, Pingitore A, Masci PG, Lombardi M. Myocardial fibrosis in isolated left ventricular non-compaction and its relation to disease severity. *Eur J Heart Fail*. 2011;13:170–6.
 45. Muhyieddeen AH, Asadourian M, Kunchakarra S, Rathod A. Recurrent ventricular tachycardia associated with lipomatous metaplasia of a myocardial scar. *BMJ Case Reports CP*. 2021;14: e240626.
 46. Suvik A, Effendy A. The use of modified Masson's trichrome staining in collagen evaluation in wound healing study. *Mal J Vet Res*. 2012;3:39–47.
 47. Brown BN, Freund JM, Han L, Rubin JP, Reing JE, Jeffries EM, Wolf MT, Tottey S, Barnes CA, Ratner BD. Comparison of three methods for the derivation of a biologic scaffold composed of adipose tissue extracellular matrix. *Tissue Eng Part C Methods*. 2011;17:411–21.
 48. Chun SY, Lim JO, Lee EH, Han MH, Ha YS, Lee JN, Kim BS, Park MJ, Yeo M, Jung B, Kwon TG. Preparation and characterization of human adipose tissue-derived extracellular matrix, growth factors, and stem cells: a concise review. *Tissue Eng Regen Med*. 2019;16:385–93.
 49. Vanhoutte D, Schellings M, Pinto Y, Heymans S. Relevance of matrix metalloproteinases and their inhibitors after myocardial infarction: a temporal and spatial window. *Cardiovasc Res*. 2006;69:604–13.
 50. Frangogiannis NG. Cardiac fibrosis: cell biological mechanisms, molecular pathways and therapeutic opportunities. *Mol Aspects Med*. 2019;65:70–99.
 51. Humeres C, Frangogiannis NG. Fibroblasts in the infarcted, remodeling, and failing heart. *JACC Basic Transl Sci*. 2019;4:449–67.
 52. Lindsey ML, Iyer RP, Zamilpa R, Yabluchanskiy A, DeLeon-Pennell KY, Hall ME, Kaplan A, Zouein FA, Bratton D, Flynn ER. A novel collagen matricryptin reduces left ventricular dilation post-myocardial infarction by promoting scar formation and angiogenesis. *J Am Coll Cardiol*. 2015;66:1364–74.
 53. Bird SD, Doevendans PA, van Rooijen MA, Brutel de la Riviere A, Hassink RJ, Passier R, Mummery CL. The human adult cardiomyocyte phenotype. *Cardiovasc Res*. 2003;58:423–34.
 54. Li J, Koikesoko C, Sugimoto J, Yoshida T, Okabe M, Nikaido T. Human amnion-derived stem cells have immunosuppressive properties on NK cells and monocytes. *Cell Transplant*. 2015;24:2065–76.
 55. Miki T. Stem cell characteristics and the therapeutic potential of amniotic epithelial cells. *Am J Reprod Immunol*. 2018;80: e13003.
 56. Hu S, Wang Z, Jin C, Chen Q, Fang Y, Jin J, Chen J, Lu L, Tian H, Xu J, et al. Human amniotic epithelial cell-derived extracellular vesicles provide an extracellular matrix-based microenvironment for corneal injury repair. *J Tissue Eng*. 2022. <https://doi.org/10.1177/20417314221122123>.
 57. Akle CA, Adinolfi M, Welsh KI, Leibowitz S, McColl I. Immunogenicity of human amniotic epithelial cells after transplantation into volunteers. *Lancet*. 1981;2:1003–5.
 58. Zhang Q, Lai D. Application of human amniotic epithelial cells in regenerative medicine: a systematic review. *Stem Cell Res Ther*. 2020;11:439.
 59. Whittaker P, Boughner DR, Kloner R. Analysis of healing after myocardial infarction using polarized light microscopy. *Am J Pathol*. 1989;134:879.
 60. Hu C, Liu W, Long L, Wang Z, Zhang W, He S, Lu L, Fan H, Yang L, Wang Y. Regeneration of infarcted hearts by myocardial infarction-responsive injectable hydrogels with combined anti-apoptosis, anti-inflammatory and pro-angiogenesis properties. *Biomaterials*. 2022;290: 121849.
 61. Talman V, Ruskoaho H. Cardiac fibrosis in myocardial infarction-from repair and remodeling to regeneration. *Cell Tissue Res*. 2016;365:563–81.
 62. Putra MA, Alwi I, Soetisna TW, Sandora N, Busro PW, Fitri NA, Kusuma TR. Remodeling in early myocardial infarction: alteration of extracellular matrix; Collagen-1, Collagen-3, α -SMA, and α -Actinin in Porcine heart model. *Bali Medical Journal*. 2023;12:2721–8.
 63. Hanna A, Shinde AV, Li R, Alex L, Humeres C, Balasubramanian P, Frangogiannis NG. Collagen denaturation in the infarcted myocardium involves temporally distinct effects of MT1-MMP-dependent proteolysis and mechanical tension. *Matrix Biol*. 2021;99:18–42.
 64. Ma Y, Chen Y, Yang Y, Chen B, Liu D, Xiong Z, Zhang C, Dong Y. Proteasome inhibition attenuates heart failure during the late stages of pressure overload through alterations in collagen expression. *Biochem Pharmacol*. 2013;85:223–33.
 65. Hou L, Guo J, Xu F, Weng X, Yue W, Ge J. Cardiomyocyte dimethylarginine dimethylaminohydrolase1 attenuates left-ventricular remodeling after acute myocardial infarction: involvement in oxidative stress and apoptosis. *Basic Res Cardiol*. 2018;113:1–12.
 66. Khodayari S, Khodayari H, Amiri AZ, Eslami M, Farhud D, Hescheler J, Nayernia K. Inflammatory microenvironment of acute myocardial infarction prevents regeneration of heart with stem cells therapy. *Cell Physiol Biochem*. 2019;53:887–909.
 67. Li Y, Hiroi Y, Liao JK. Notch Signaling as an Important Mediator of Cardiac Repair and Regeneration After Myocardial Infarction. *Trends Cardiovasc Med*. 2010;20:228–31.
 68. Pinto AR, Ilinykh A, Ivey MJ, Kuwabara JT, D'Antoni ML, Debuque R, Chandran A, Wang L, Arora K, Rosenthal NA. Revisiting cardiac cellular composition. *Circ Res*. 2016;118:400–9.

69. Chang T, Liu C, Yang H, Lu K, Han Y, Zheng Y, Huang H, Wu Y, Song Y, Yu Q, Shen Z, Jiang T, Zhang Y. Fibrin-based cardiac patch containing neuregulin-1 for heart repair after myocardial infarction. *Colloids Surf B*. 2022;220: 112936.
70. Shinde AV, Frangogiannis NG. Fibroblasts in myocardial infarction: a role in inflammation and repair. *J Mol Cell Cardiol*. 2014;70:74–82.
71. PARK, J. & TALLQUIST, M. D. 2018. Cardiac Fibroblast. In: VASAN, R. S. & SAWYER, D. B. (eds.) *Encyclopedia of Cardiovascular Research and Medicine*. Oxford: Elsevier.
72. Daskalopoulos EP, Janssen BJ, Blankesteijn WM. Myofibroblasts in the infarct area: concepts and challenges. *Microsc Microanal*. 2012;18:35–49.
73. Shinde AV, Humeres C, Frangogiannis NG. The role of α -smooth muscle actin in fibroblast-mediated matrix contraction and remodeling. *Biochimica et Biophysica Acta (BBA) Molecular Basis of Disease*. 2017;1863:298–309.
74. Reksodiputro M, Pratama G, Wiweko B, Kusumawardhani E, Rahayu D, Nauli R, Martin V, Sandora N. Incubation of platelet-rich fibrin matrix with mesenchymal stem cells improves matrix stiffness. *Int J Appl Pharm*. 2020;12:111–6.
75. Sandora N. Regeneration of decellularised tendon by human mesenchymal stem cells in response to uniaxial tensile strain. Leeds: University of Leeds; 2016.
76. Raina N, Rani R, Gupta M. Angiogenesis: aspects in wound healing. In: Chatterjee S, editor. *Endothelial signaling in vascular dysfunction and disease*. London: Elsevier; 2021.
77. Bollini S, Silini AR, Banerjee A, Wolbank S, Balbi C, Parolini O. Cardiac restoration stemming from the placenta tree: insights from fetal and perinatal cell biology. *Front Physiol*. 2018;9:385.
78. Kofler S, Nickel T, Weis M. Role of cytokines in cardiovascular diseases: a focus on endothelial responses to inflammation. *Clin Sci*. 2005;108:205–13.
79. Ahmad F, Banerjee SK, Lage ML, Huang XN, Smith SH, Saba S, Rager J, Conner DA, Janczewski AM, Tobita K. The role of cardiac troponin T quantity and function in cardiac development and dilated cardiomyopathy. *PLoS ONE*. 2008;3: e2642.
80. Nakao K, Minobe W, Roden R, Bristow MR, Leinwand LA. Myosin heavy chain gene expression in human heart failure. *J Clin Invest*. 1997;100:2362–70.
81. GENE 2023. KIT proto-oncogene, receptor tyrosine kinase [Homo sapiens (human)]. Bethesda (MD): National Library of Medicine (US), National Center for Biotechnology Information
82. Costa A, Balbi C, Garbati PR, Lodder K, van Herwaarden T, Turturo S, Palmeri A, de Biasio P, Barile L, Goumans M, Smits AM, Bollini S. The human amniotic fluid stem cell secretome exerts cardio-active paracrine potential for myocardial repair and regeneration. *Cytotherapy*. 2020;22:S171.
83. Wolfien M, Klatt D, Salybekov AA, Li M, Komatsu-Horii M, Gaebel R, Philippou-Massier J, Schrinner E, Akimaru H, Akimaru E, David R, Garbade J, Gummert J, Haverich A, Hennig H, Iwasaki H, Kaminski A, Kawamoto A, Klopsch C, Kowallick JT, Krebs S, Nesteruk J, Reichenspurner H, Ritter C, Stamm C, Tani-Yokoyama A, Blum H, Wolkenhauer O, Schambach A, Asahara T, Steinhoff G. Hematopoietic stem-cell senescence and myocardial repair—coronary artery disease genotype/phenotype analysis of post-MI myocardial regeneration response induced by CABG/CD133+ bone marrow hematopoietic stem cell treatment in RCT PERFECT Phase 3. *EBioMedicine*. 2020;57: 102862.
84. de Sena-Tomás C, Aleman AG, Ford C, Varshney A, Yao D, Harrington JK, Saúde L, Ramialison M, Targoff KL. Activation of Nkx2.5 transcriptional program is required for adult myocardial repair. *Nat Commun*. 2022;13:2970.
85. Anderson DJ, Kaplan DI, Bell KM, Koutsis K, Haynes JM, Mills RJ, Phelan DG, Qian EL, Leitoguinho AR, Arasaratnam D, Labonne T, Ng ES, Davis RP, Casini S, Passier R, Hudson JE, Porrello ER, Costa MW, Rafii A, Curl CL, Delbridge LM, Harvey RP, Oshlack A, Cheung MM, Mummery CL, Petrou S, Elefanty AG, Stanley EG, Elliott DA. NKX2-5 regulates human cardiomyogenesis via a HEY2 dependent transcriptional network. *Nat Commun*. 2018;9:1373.
86. Lakin ND, Jackson SP. Regulation of p53 in response to DNA damage. *Oncogene*. 1999;18:7644–55.
87. Karimian A, Ahmadi Y, Yousefi B. Multiple functions of p21 in cell cycle, apoptosis and transcriptional regulation after DNA damage. *DNA Repair (Amst)*. 2016;42:63–71.
88. Anversa P, Cheng W, Liu Y, Leri A, Redaelli G, Kajstura J. Apoptosis and myocardial infarction. *Basic Res Cardiol*. 1998;93:8–12.
89. Hunter AL, Zhang J, Chen SC, Si X, Wong B, Ekhterae D, Luo H, Granville DJ. Apoptosis repressor with caspase recruitment domain (ARC) inhibits myogenic differentiation. *FEBS Lett*. 2007;581:879–84.
90. MURRAY, T. V., MCMAHON, J. M., HOWLEY, B. A., STANLEY, A., RITTER, T., MOHR, A., R., Z. & FEARNHEAD, H. O. 2008. A non-apoptotic role for caspase-9 in muscle differentiation. *J Cell Sci*, 121.
91. Solozobova V, Blattner C. p53 in stem cells. *World J Biol Chem*. 2011;2:202–14.

Publisher's Note

Springer Nature remains neutral with regard to jurisdictional claims in published maps and institutional affiliations.